Spring 2020

A Post-Impact Behavior of Platelet-Based Composites Produced by Compression Molding

Christopher Eugene Ervin Volle
Old Dominion University, volle593@gmail.com

A POST-IMPACT BEHAVIOR OF PLATELET-BASED COMPOSITES PRODUCED BY COMPRESSION MOLDING

by

Christopher Eugene Ervin Volle
B.S. December 2016, University of Nebraska–Lincoln

A Thesis Submitted to the Faculty of
Old Dominion University in Partial Fulfillment of the Requirements
for the Degree of

MASTER OF SCIENCE

MECHANICAL AND AEROSPACE ENGINEERING

OLD DOMINION UNIVERSITY
May 2020

Approved by:

Oleksandr Kravchenko (Director)

Mileta M.Tomovic (Member)

Tian-Bing Xu (Member)

ABSTRACT

A POST-IMPACT BEHAVIOR OF PLATELET-BASED COMPOSITES PRODUCED BY COMPRESSION MOLDING

Christopher Eugene Ervin Volle
Old Dominion University, 2020
Director: Dr. Oleksandr Kravchenko

Prepreg-based Platelet Molded Compounds (PPMCs) are quickly becoming a widely used method for creating structural components in the aerospace and automotive industries. The discontinuous nature of the platelets used allow good formability of both complex and basic structural components; from seats on commercial airplanes to outer panels of vehicles.

This thesis will look at an important research question of these composites: how PPMCs behave under dynamic loading, e.g. impact and post-impact behavior. Impact is analyzed using recorded force and velocity data to find the absorbed energy. Digital image correlation is used with compression after impact testing to study the propagation of damage in the material with the initial damage present due to impact loading. Residual strengths from compression after impact tests yield a way to evaluate the associated strength knockdown due to the extent of damage within a material. The role of the platelet geometry, by varying platelet length, was evaluated. This work provides a greater insight into the behavior of the prepreg platelet molding compound under impact and post-impact behavior, which is important for understanding structure-property relationships in these composites when subjected to various loading conditions.

Dedicated to Tobias – and to the notion that life will lead you to where you are supposed to be, if only you listen.

ACKNOWLEDGEMENTS

I would like to thank Dr. Kravchenko for taking me under his wing and for providing his knowledge and support. Special thanks go to Dr. Kravchenko and the ODU Mechanical and Aerospace Engineering department for funding assistance. Thanks to my committee for their support. Thanks to Wade Jackson for his help and support in specimen testing. Thanks to everyone in the composites research lab for their instruction and knowledge of materials and fabrication. To Jonathan Tan, for his help in grammar and general editing. To Michelle Rodio, my graduation buddy and best friend for kicking my butt in gear. Special thanks go to my friends and family for their continued support throughout all of my years of schooling. To David Glass, Su-Yuen Hsu, and everyone at NASA Langley Research center for their professional insight, guidance, knowledge, and incredible opportunities they have given me. Finally, thank you to my mentors, Karen Stelling and Nathanael Miller, for I would not be where I am today without your professional guidance and personal friendship.

TABLE OF CONTENTS

LIST OF TABLES

LIST OF FIGURES

CHAPTER 1

INTRODUCTION

Composites have been around for many years, though carbon fiber composites have quickly become the industry standard for lightweight structures due to their strength, formability, and versatility [1]. These materials are being constantly studied in order to better their properties, behavior, and find new uses for them. This paper will attempt to chip away at what is still unknown about composites by exploring compression after impact of a specific material system of composites.

Fiber length contributes greatly to both the properties and the structures capable of being manufactured. Short fibers are easily molded into complex shapes but have weaker material properties, which are governed by the properties of the matrix. Continuous fiber composites have greater strength but are more difficult to manufacture due to the need for very long sheets, which are inherently necessary for them to be continuous fibers, as shown in Fig. 1. Long fiber composites, such as those in platelet-based composites, are a good trade-off between continuous and short fiber composites.

Prepreg platelet molded compounds are versatile, as they can be molded into almost any shape. This allows parts to be manufactured faster, cheaper, and stronger than the same part if it was made of aluminum [2]. Today, platelet-based composites are used to make replacements for secondary structures; for example, brackets and airplane seats, such as the one shown in Fig. 2. Platelet-based composites are comprised of prepreg-based platelets of fibers aligned in one direction across the platelet. It is important these platelets already

contain prepreg. If the platelets did not contain prepreg, they would cease to retain their tape-like shape and become a pile of dry fibers. It would be difficult to add epoxy to these free fibers without causing a preference in direction for the material properties, as the epoxy flowing between the fibers would viciously drag the fibers to align them in the direction of the flow. This object is made entirely of compression molded composites, in two pieces. If the composite part were composed of a metal such as aluminum, the part would likely be thicker to forgo the machining cost of the struts. This would also likely take weeks to machine. Instead, the part is made in a couple of hours, as the platelets are capable of filling all the gaps of the mold, given the right pressure.

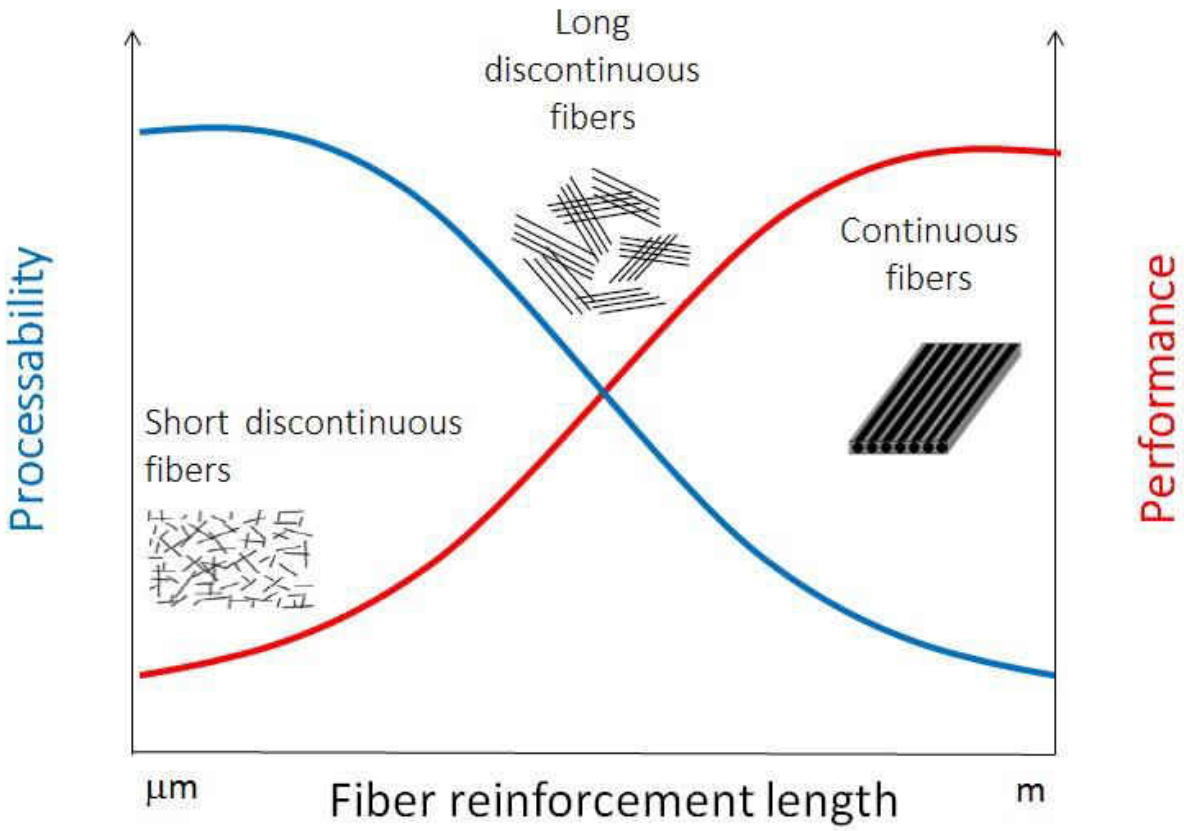

Fig. 1: Correlation between fiber length, processability, and performance.

The morphology of platelet molded composites, as will be discussed in this paper, is stochastic, and has been characterized previously in papers by Feraboli [3], [4]. It is possible to vary the platelet width, length, and thickness as well. The changes in these dimensions have an effect on the strength of materials. Generally, an increase in length also have a positive effect on the properties; conversely, increasing thickness has a negative effect [5], [6], [7]. Width remained constant in this experiment and modeling. If the platelets are long, the platelets are more capable of load transfer to other platelets. This paper will explore a variation in platelet length.

Fig. 2: Airplane seat made of prepreg platelet molded composites at ACCE 2019.

Photo credit: Dr. Kravchenko.

In Kravchenko's paper, the writers define several fracture modes of platelets as platelet rupture and/or disbond. The probability of one failure occurring over the other depends on platelet size, preferring to rupture or tear as the platelet increases in length.

A major reason why it is necessary to research and understand these composites can be seen in Fig. 3, a door of the new Toyota Prius. Every year, 40,000 people die as the result of vehicular injury [8], [9]. While this is not usually the fault of a certain material, this platelet molded composite material could present new dangers in car crashes. Even though advancements in materials allow new uses, they also present new potential dangers. Vehicles are unsafe modes of travel, so as more prepreg platelet molded composite parts are used in vehicles, impact with these composites become more likely. In impact, these composites become sharp, brittle edges, which could cause severe harm in a collision. Studying the fracture of these composites can allow better design of structure to decrease the likelihood of injury, and allow the industry to understand just how much damage these materials can take before they become a danger. Compression After Impact (CAI) testing is used to determine the impact resistance of the material.

CAI uses impact to investigate damage occurring in materials [10]. In this testing, some material is used as a control. The control is a pristine, unimpacted material used for comparison with impacted specimens. Low-velocity impact testing is conducted by suspending a mass at a specific height to obtain a certain amount of impact energy, due to the direct relationship between potential and kinetic energy [11], [12]. This obtains a residual strength of the material after impact as a function of impact energy. While this has been tested for continuous fiber material, this has not been an area of study for

discontinuous fiber composites. Some testing of reinforcements using titanium has also been explored [13].

Fig. 3: Rear door of the new Toyota Prius, made of prepreg platelet molded composites. Photo credit: Dr. Kravchenko.

Compression testing of composites is widely studied, especially for continuous fibers. It is possible to tailor the arrangement of these composites to get good properties for different directions. In-plane properties have been getting better for years, though out-of-plane properties are primarily relying on the properties of the matrix.

Ghelli explored the effect of layup direction on the residual strength through CAI testing [14]. In this paper, delamination area was explored as a function of impact energy. A strong correlation was found for impact energy and energy absorbed. Force vs time was explored, finding a higher contact force and contact time for a greater impact energy. Force vs displacement was presenting, showing a correlation between impact energy and maximum displacement. Compression results for these continuous fiber composites showed reduced residual strength, given a higher impact energy.

Modeling of CAI for composite laminates was conducted in a paper by Wei Tan [15]. Force vs time, force vs displacement, delamination envelopes were created for these models. Models primarily predicted matrix damage and delaminations as a result of impact. Numerical simulations correlated well with experimental results.

Delamination area is the driving factor in CAI, compared to layup orientation [16]. Freitas found that as impact energy increases, so does delamination area [16]. Delamination area is the projection on a specimen plane of delaminated area, considering all delamination interfaces. It is not the total area per interface.

The strength of composites with holes in them have been widely explored [17], [18], [19], [20], [21]. Results show the fiber discontinuity is a driving factor in increased stress concentrations around the hole. In discontinuous fiber materials, platelets are likely to disbond/delaminate, rather than rupture. Though not explored in this paper, load transfer mechanisms may be similar, but failure in impacted platelet-based specimens is different by use of disbond rather than fiber fracture.

ASTM D7137 CAI Fixture was designed for 4 mm thick specimens with a length and width of 6" and 4", respectively [22]. Though the device was likely designed to provide a minor clamping force to the edges, it appears to provide a minor clamping force to the top and bottom of the specimen, but allows a simple support at the edges.

Acceptable material-failure modes can be seen in Fig. 4 [22]. Starting at the top left and working clockwise, these are: lateral through the damage, lateral through the gauge, splitting through the damage, widthwise delamination growth through damage to the edge, and lengthwise delamination to the edge through the damage. The problem with the device

is that thinner laminates are not possible. Using the ASTM device, the laminate buckles for any laminate thickness less than 4 mm.

A paper by Remacha proposed a new device to replace the ASTM Standard [23]. The proposed device was similar to the ASTM device, except this device allowed for thinner laminates. Laminates of 2.944 mm tested with the new device showed no difference in ultimate strength compared to 4 mm thick laminates tested with the ASTM device, however 1.472 mm laminates had a strength (due to buckling) of 30% less strength. This lower strength was due to buckling in the thin laminate. Remacha used struts to prevent buckling, though a section in the middle was without struts to avoid interference with damage.

The laminates used in this paper average 1.7 mm. Laminates that were thinner than usual were chosen because the application of these morphologies. Typical applications include airplane seats and car panels where parts are difficult to machine. Plastic can be used, but use of carbon fiber composites is being explored due to their increased mechanical properties. Composites that are 4 mm and thicker are not used for these applications as it would make the part too heavy. Therefore, behavior of thinner laminates must be explored in case there is a difference in behavior from ASTM-recommended testing standards.

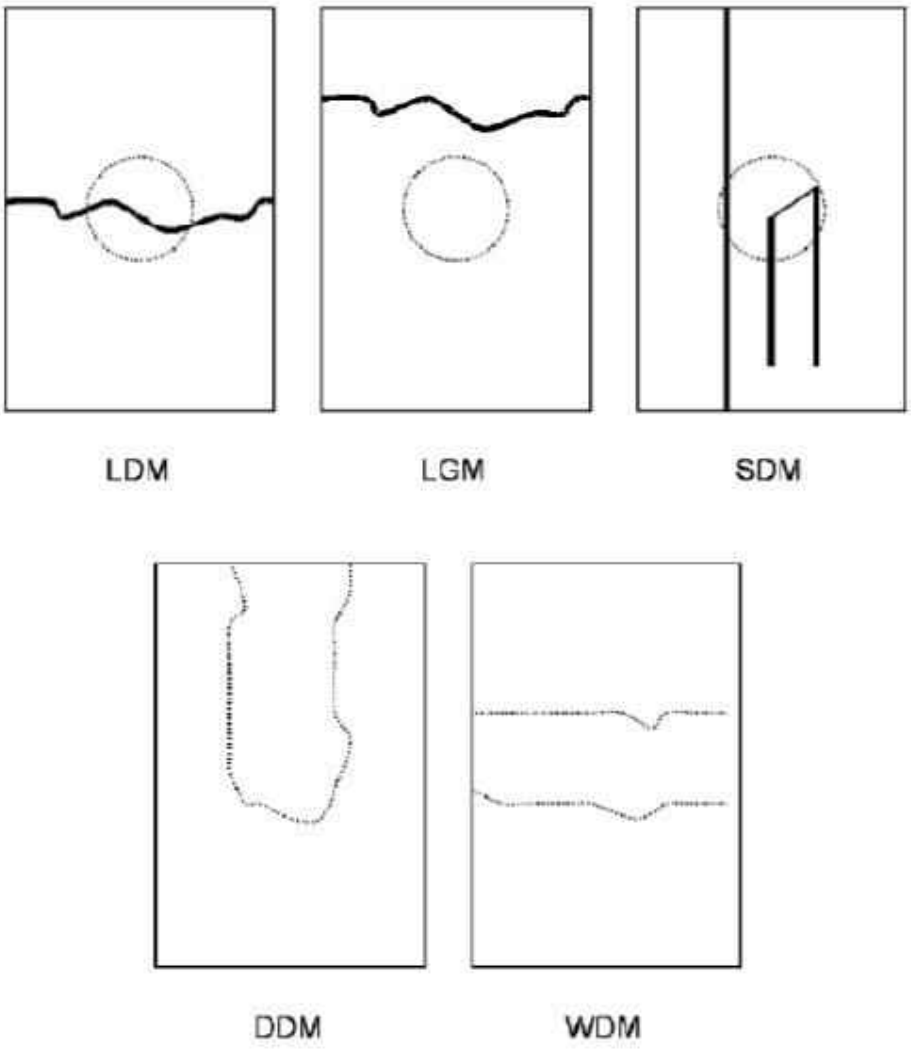

Fig. 4: Acceptable failure modes, as depicted by the ASTM D7137 Standard.

Another design for CAI in thin materials was used by Sanchez-Saez [24]. The boundary conditions used a clamping force on the edges of the specimen, except for a small section in the middle to allow for shrinking of the specimen due to compression. A middle section was not clamped to avoid interference with the impacted section of the specimen. Similar to other papers, Sanchez-Saez found an increase in impact energy correlated to a decrease in ultimate strength.

Even though the papers above attempted to mitigate buckling of the material by way of the fixture design, in the end it was unavoidable for thin materials. It may be possible to explore the use of honeycomb core as a way to diminish global buckling, though the core may introduce unseen effects [25]. Several references are used in the calculation of buckling in this paper [26], [27], [28]. All designs described above were considered for the final design of the compression fixture. Design requirements were determined, resulting in a fixture design for fabrication. The final design allowed for use of Digital Image Correlation (DIC) during compression of the specimen, using a window to both allow for the DIC and prevent interaction with the damaged section of the material.

This thesis will investigate the residual strength of thin, platelet-based composites after impact at various energy levels. Quasi-isotropic 60°, 25.4 mm platelet, and 12.7 mm platelet composites will be presented.

CHAPTER 2

METHODOLOGY

This paper seeks to describe the relationship between platelet length-to-width ratio and residual strength after impact compared to pristine specimens. To do this, a quasi-isotropic 60° (Quasi-60) $[0/_{+}60/_{-}60]_{2s}$ will be used as a control for all experiments across materials and impact energy levels. The setup will be discussed, followed by the manufacturing and testing of materials.

2.1 EXPERIMENT SETUP

In Navarro's paper, CAI of a continuous fiber composite is explored for a quasi-isotropic $[0/_{+}45/_{-}45/90]_{s}$ composite layup. This provided a laminate thickness of between 1.5 and 2.2 mm. The composite tape material used in this thesis is thicker than the material used in Navarro, so a Quasi-60 was to be used to obtain a similar thickness. Given layup plays less of a roll in residual strength than delamination area, it was determined this would be a reasonable substitute for the experiment. For further comparison with Navarro, similar specimen size of 76 mm by 76 mm was selected.

Preliminary testing showed 25.4 mm and 12.7 mm platelets would give interesting results. 6.4 mm platelets were not explored due to the need for a lighter impactor weight, which was not possible with the equipment.

Due to material variability, at least two panels were made per type, with the intention of having at least 5 specimens per material and impact energy. Given impact energies of 0, 2.5,

5, and 10 J, and 3 material types, this meant 60 specimens total. In reality, some materials could not withstand some energy levels and equipment variability meant this did not necessarily occur. A table detailing how many specimens were tested for each energy level and material type can be found in Table I. Only 55 specimens were tested, though 5 specimens had bad or corrupted data.

TABLE I: Number of specimens tested per material per energy level.

Impact Energy	Quasi-60	25.4 mm	12.7 mm
0	7	5	6
2.5	5	5	6
5	6	5	3
10	3	3	1

In order to combat material scatter and ensure properties did not vary plate to plate, specimens were made in batches. The largest reasonable plate was 254 mm by 254 mm due to the limits of the heated press. Given a specimen size of 76 mm by 76 mm, nine specimens were available per batch. This size did not allow for struts on the CAI fixture, as some damage spread too close to edges to make struts useful. Instead, a window was fashioned for use in DIC.

2.2 MATERIAL MANUFACTURING

The material used is Hexel IM7-8552 [29]. This material comes in large rolls of carbon fiber tape. The tape is made of continuous fibers held together by epoxy resin, and is the same material used on NASA Langley's automated fiber-placement robot, ISAAC.

2.2.1 CONTINUOUS FIBER MATERIAL: QUASI-60 LAYUP

To make the Quasi-60 layup, strips were laid down adjacent to each other to form a layer with fibers all in one direction. Subsequent layers were angled to form layers with fibers at 60 ° and -60 ° to form a $[0/_{+}60/_{-}60]_{2S}$. This panel was then cured in an autoclave using the cure cycle in Table II.

2.2.2 DISCONTINUOUS FIBER MATERIALS: 25.4 mm AND 12.7 mm PLATELETS

This composite is chopped using a guillotine-style paper cutter to form 25.4 mm and 12.7 mm platelets which are 6.4 mm wide. The material cut totaled to about 165 g per panel and was placed into a 254 mm by 254 mm mold, as seen in Fig. 5 and Fig. 6. The chopped fibers were then cured using the recipe in Table II using the heated press-clave in Fig. 7.

TABLE II: Manufacturing Recipe.

Temperature °C	**Duration, mins**	**Pressure, psi**	
		Quasi-60	**Chopped**
108	30	20	10
108	35	80	1,500
180	120	80	1,500

Both types of panel were then cut into 76 mm by 76 mm specimens using a waterjet machine and measured in all dimensions in preparation for impact and compression testing. Figure 8 shows a finished 25.4 mm plate ready for waterjet cutting.

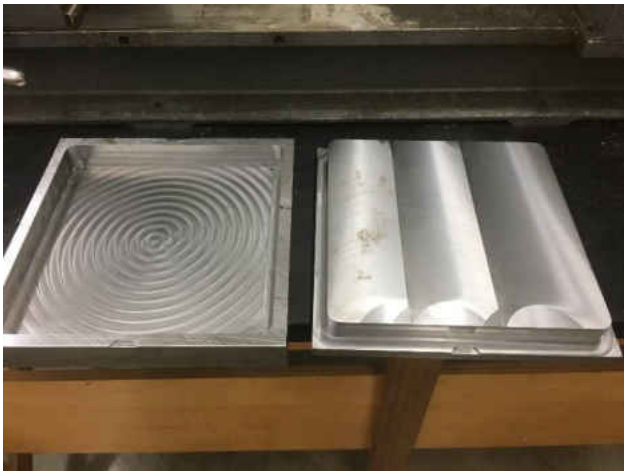

Fig. 5: Mold used to make 254 mm plate.

Fig. 6: Mold used to make 254 mm plate filled with platelets.

Fig. 7: Heated press used for making prepreg platelet molded composites.

Fig. 8: Panel of 25.4 mm platelet material in the waterjet. The panel is ready to be cut into 9 specimens for testing.

2.3 TESTING

Here, impact and compression testing methods used in this paper will be described.

2.3.1 IMPACT TESTING

Impact testing was performed at the NASA Langley Research Center using their low-velocity drop tower located in Building 1205. The setup in question utilized a 3-meter tall tube containing an impactor, as shown in Fig. 9. This impactor was equipped with a force sensor and a velocity gate in order to measure the impact energy and impact velocity, respectively. Data was saved to an oscilloscope, reading at 200 kHz. Specimens of all materials were tested at 2.5 J, 5 J, and 10 J, though some 12.7 mm specimens were tested at 1.25 J. A simple energy balance was used to find an impact energy of 5 J at approximately 0.305 m in height, given an impactor weight of about 3.8 lbs. A minor increase in height was added to account for friction in the tube.

The tip of the impactor is a 15.88 mm hemisphere. The impact fixture is a fixed-edge support for the specimen using two aluminum plates. Force was measured through a load cell behind the impactor tip. The object clamped with the vice grip is the velocity gate sensor used to measure the time of flight of a velocity gate on the side of the impactor. Data recorded was used to calculate the impact energy absorbed by the material.

$$v_o = \sqrt{2E/M} \tag{1}$$

$$H = \frac{E}{Mg} \tag{2}$$

$$x(t) = x_o + \int_0^t \left[v_o - \int_0^t \frac{F(\zeta) - P}{m} d\zeta \right] d\tau \tag{3}$$

$$E(t) = \int_0^t F(\tau) \left[v_o - \int_0^t \frac{F(\zeta) - P}{m} d\zeta \right] d\tau \tag{4}$$

Fig. 9: Impactor setup.

2.3.2 COMPRESSION TESTING

All specimens were then compression tested on an MTS compression machine using a 300 kN load cell. Specimens were tested at a rate of 0.5 mm/min. Strain data was not recorded, though DIC was used. A fixture was designed to interface with the platens of the MTS and hold the specimens for compression testing, as shown in Fig. 10. The fixture was designed to reduce bending, buckling, brooming, and pinching of the specimen by clamping down on the edges of the specimen.

Brooming is a phenomenon where force is applied to the specimen and the edges of the specimen fray, spreading out to resemble the end of a broom, as shown in Fig. 11(a). This phenomenon was avoided by designing the compression fixture to apply an out-of-plane force to these edges. Pinching can occur between the top and bottom pieces of the fixture during compression. When this occurs, the specimen's sides bulge out as a result of delamination. Extreme pinching of the specimen was avoided by rounding several edges of the fixture in contact with the specimen. Pinching was not observed in discontinuous fiber materials, though an example of pinching can be observed in Fig. 11(b).

The ASTM Standard was not used due to the size of the specimens, and because platelets are prone to end-crushing/brooming. The ASTM Standard does not do enough to prevent unacceptable failure modes for these composites, especially for discontinuous fibers which seem to have been more prone to these edge effects. The specimens needed to be comparable to Sanchez-Saez [24].

The fixture was designed to ensure evenly loaded compression of the specimens without bending or buckling by clamping all edges of the specimen. Testing showed no indications of misalignment, so guiding rods were not added to the fixture. Clamping the edges ensured

a fixed edges condition (rather than using simple supports), which assisted the specimen to resist buckling.

Fig. 10: Compression fixture.

The bending rigidity is given in Eq. 5 [27], [26]. In this equation, the material modulus, thickness, and Poisson's ratio are represented by E, t, and ν, respectively. The bending rigidity is then used with the width of the material and a critical buckling factor to find the critical buckling load per unit length, represented by b and k_c, respectively.

The critical buckling factor depends on the boundary conditions of the compressive setup. The conditions assumed clamped edges on all four sides of the specimen. The specimen area under the clamp was not assumed to be part of the specimen that could buckle, and was subtracted from the dimensions used for calculating the critical buckling loads. Using MIT's online lectures and assuming a specimen aspect ratio of about 0.8, the

critical buckling factor of approximately 11.5 was determined. Using experimentally determined moduli, buckling loads of 950 MPa, 384 MPa, and 359 MPa were determined for the pristine Quasi-60, 25.4 mm, and 12.7 mm, respectively.

(a) Brooming of the loading edge of a speci- (b) Pinching of a specimen edge. men.

Fig. 11: Undesirable failure artifacts.

$$\sigma_c = k\frac{\pi^2 E}{12(1-\nu^2)\left(\frac{b}{t}\right)^2} \tag{5}$$

CHAPTER 3

RESULTS

Presented in this section are the results of all specimen testing. An interpretation of this data is presented in the discussion. Points for a specimen type and energy not aligned vertically (such as red circles P527-050-025) were recorded to have been tested at one energy level (ex. 2.5 J), but the math shows these were tested at a different energy level (ex. 2 specimens at 1.25 J and one at 2.5 J).

3.1 FORCE VS TIME

Typically, CAI explores damage that cannot easily be seen. The 10 J specimens show evidence of too much damage, both physically and in the impact data. Specimens were not punctured, but contained a dent larger than the Barely Visible Impact Damage threshold for composite of this thickness, possibly classifying the damage as a hole due to breakage of the fibers. Even so, these results of these severely damaged specimens will be reported.

The Force–Time response of the 12.7 mm specimen at 10 J is not reported on the Force vs time graphs because the specimen was fully punctured by the impactor at the time of impact, with no rebound. The residual strength is later presented. The Force–Time response will be discussed by comparing differing impact energies for each material type, as well as comparing material types for each energy level.

3.1.1 FORCE–TIME RESPONSE: A COMPARISON OF IMPACT ENERGY

The comparison of differing impact energies for each material time is shown in Fig. 12. The response time of the Quasi-60 layup was the same for every energy level, as shown in

Fig. 12(a). Though it is difficult to discern in these images, it is worth noting the impact response of the specimens is wavy until about 80% of the maximum contact force is reached, after which the response is sharp. The 10 J specimen response has a sharp drop after 800 lbf contact force, after which it imitates the response of the 5 J specimens.

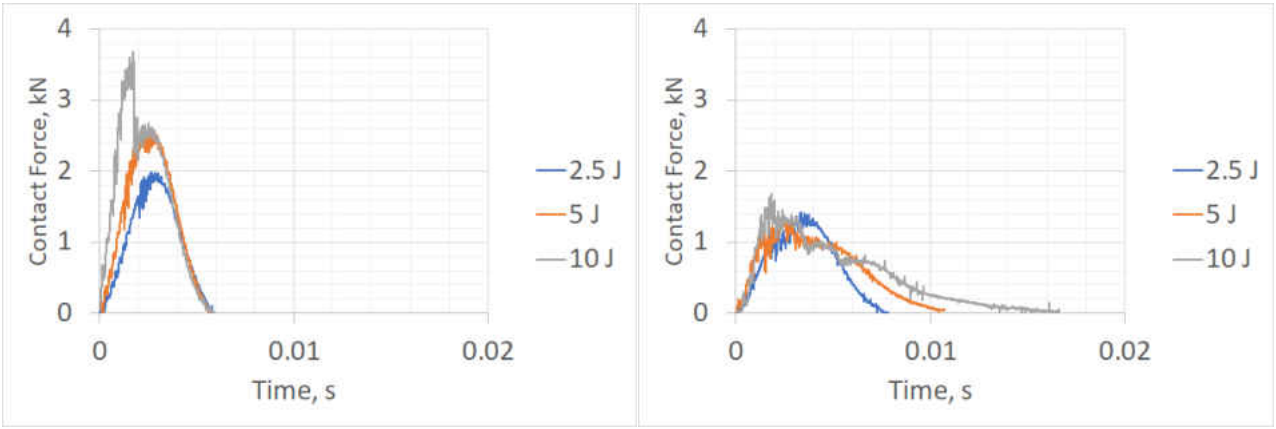

(a) Q60. (b) 25.4 mm.

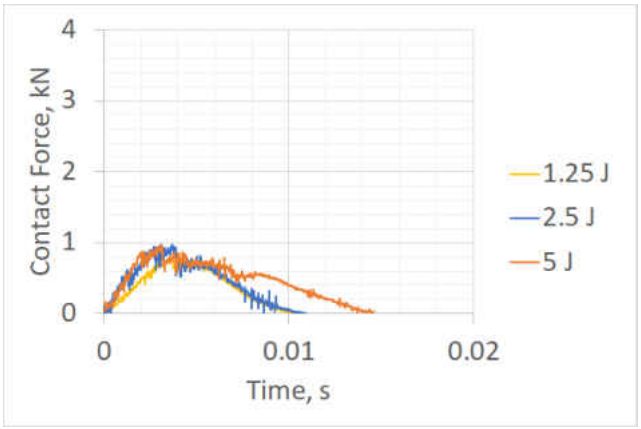

(c) 12.7 mm.

Fig. 12: Force vs time comparison of impact energy for all materials.

Compared to the Quasi-60, the responses of the 25.4 mm and 12.7 mm specimens are irregular, as shown in Fig. 12(b) and Fig. 12(c), respectively. In both materials, the response time increases with each energy level. Similar to the Quasi-60 specimen tested at 10 J, there

are discontinuous specimens where there is a drop in the contact force followed by an increase of the response. This occurrence is more frequent as the applied impact energy increases, and may be due to delaminations propagating in the material. It is difficult to confirm this due to the inability to measure the delaminations during impact, though could be shown with computational modeling of these tests.

3.1.2 FORCE–TIME RESPONSE: A COMPARISON OF MATERIALS

A comparison of the Force–Time responses for all sample configurations at 2.5 J, 5 J, and 10 J can be seen in Fig. 13. Graphs are coordinated to have similar axes for easy comparison between energy levels. The response time increases with decreasing fiber length. Discontinuous materials have a more flat, long, and lingering response, whereas the continuous fiber material is uniform and typically symmetric.

The response for the 2.5 J specimens was extremely similar for all materials, the difference being that curves for shorter fibers were squished down and stretched out. This can be observed in Fig. 13(a). Otherwise, the general shape, a bell curve, was essentially the same.

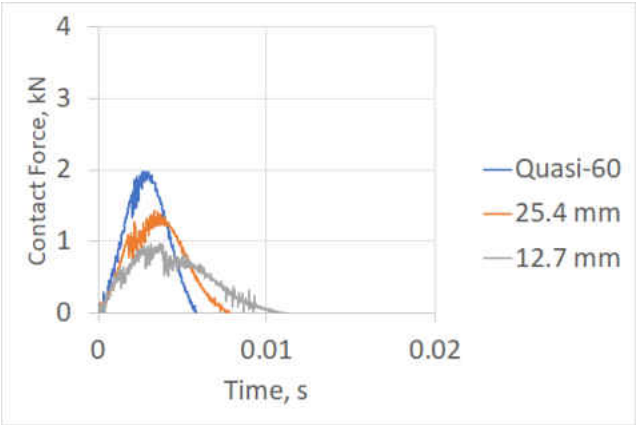

(a) 2.5 J.

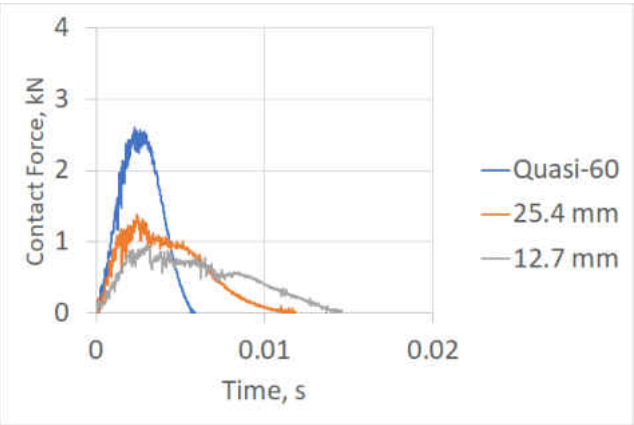

(b) 5 J.

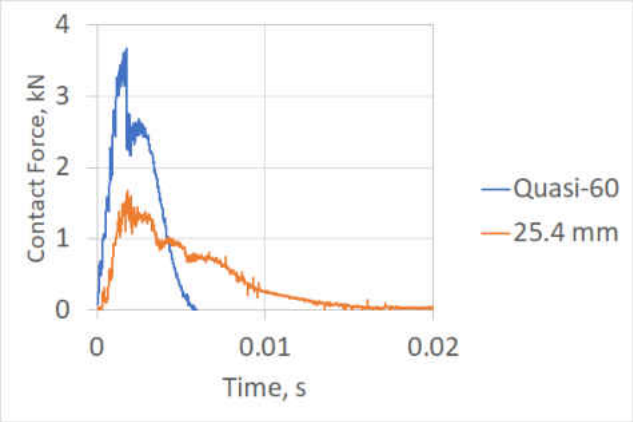

(c) 10 J.

Fig. 13: Contact Force vs time for comparison between materials.

3.2 FORCE VS DISPLACEMENT

This section will discuss Force vs Displacement results of the impact testing. These charts are a way to show energy absorbed by the material due to impact. If there was no energy loss of the material, the unload slope would be approximately equal to the loading slope. Energy absorption is observed when the force–displacement curve visually creates a loop. Smooth oscillations indicate elastic response of the material, whereas jagged portions are

another indicator of energy loss in the material. Results proved similar to those presented in Ghelli [14].

The certain axes have been generalized to better show relative force or displacement between material types and energy levels. Color has been kept constant for each energy level or materials between graphs, depending on the section.

3.2.1 FORCE–DISPLACEMENT RESPONSE: A COMPARISON OF IMPACT ENERGY

Force vs displacement for Quasi-60, 25.4 mm, and 12.7 mm specimens at various energy levels can be seen in Fig. 14. In every graph, the area contained in the loop created by the material response grows larger with increasing impact energy. The displacement depth also increases with increasing impact energy for every material. The only specimen that seems to have taken very little or no damage is the Quasi-60 specimen impacted with 2.5 J of energy. It is not difficult to discern impact damage occurred in all other specimens, as indicated by the nonlinear unloading slope.

The 12.7 mm specimens do not allow a contact force greater than 200 lbf, whereas 25.4 mm specimens do not allow more than about 350 lbf. Little front-surface damage was visible in all materials tested below 5 J, though several cracks/delaminations could usually be observed on the back surface. All materials 5 J and up showed a surface dent at the location of impact, as well as significant damage on the back side of the specimen.

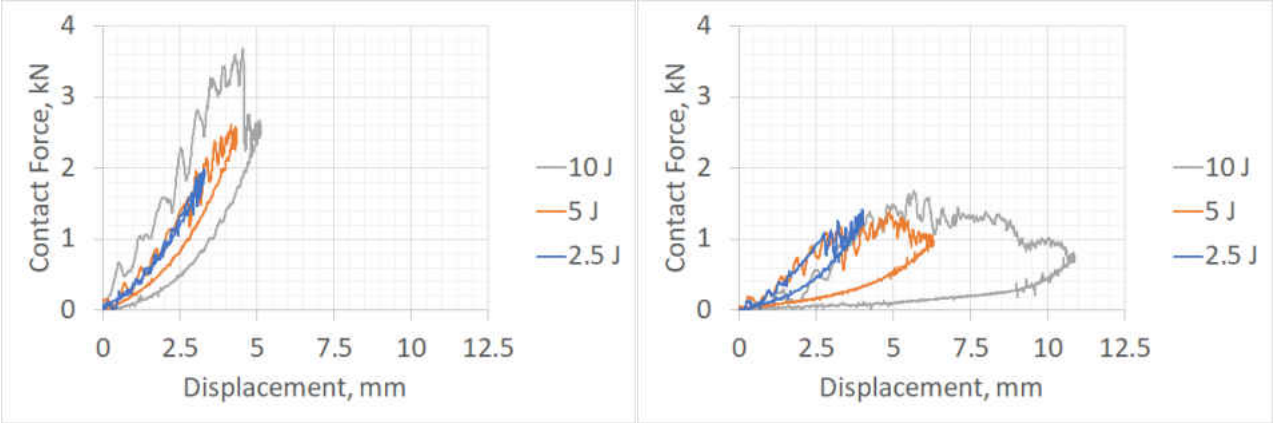

(a) Q60. (b) 25.4 mm.

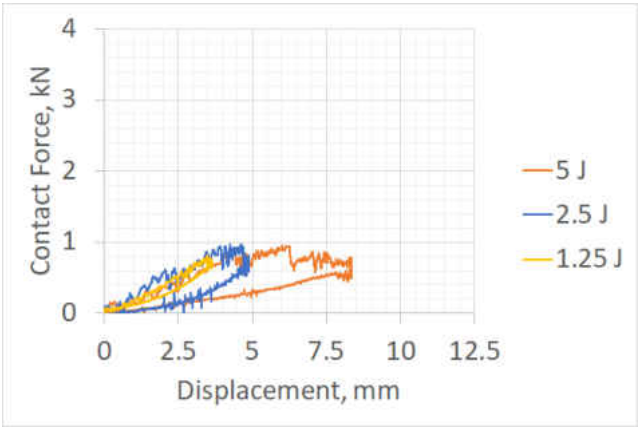

(c) 12.7 mm.

Fig. 14: Force vs Displacement comparison of impact energy for all materials.

3.2.2 FORCE–DISPLACEMENT RESPONSE: A COMPARISON OF MATERIALS

A Force–Displacement of the different impact testing for 1.25 J, 2.5 J, 5 J, and 10 J can be found in Fig. 15. Graph axes have been generalized for better comparison between energy levels.

It is apparent more energy was absorbed as fiber length decreased. This is shown by the progressively increasing area contained within the loops as fiber length decreases. It can also be seen that displacement increases as fiber length decreases. The Quasi-60 has the smallest displacement and the highest contact force, whereas the 12.7 mm specimen has the

largest displacement and smallest maximum contact force. There is no discernible damage incurred in the Quasi-60 specimen when looking at the response in Fig. 15(a).

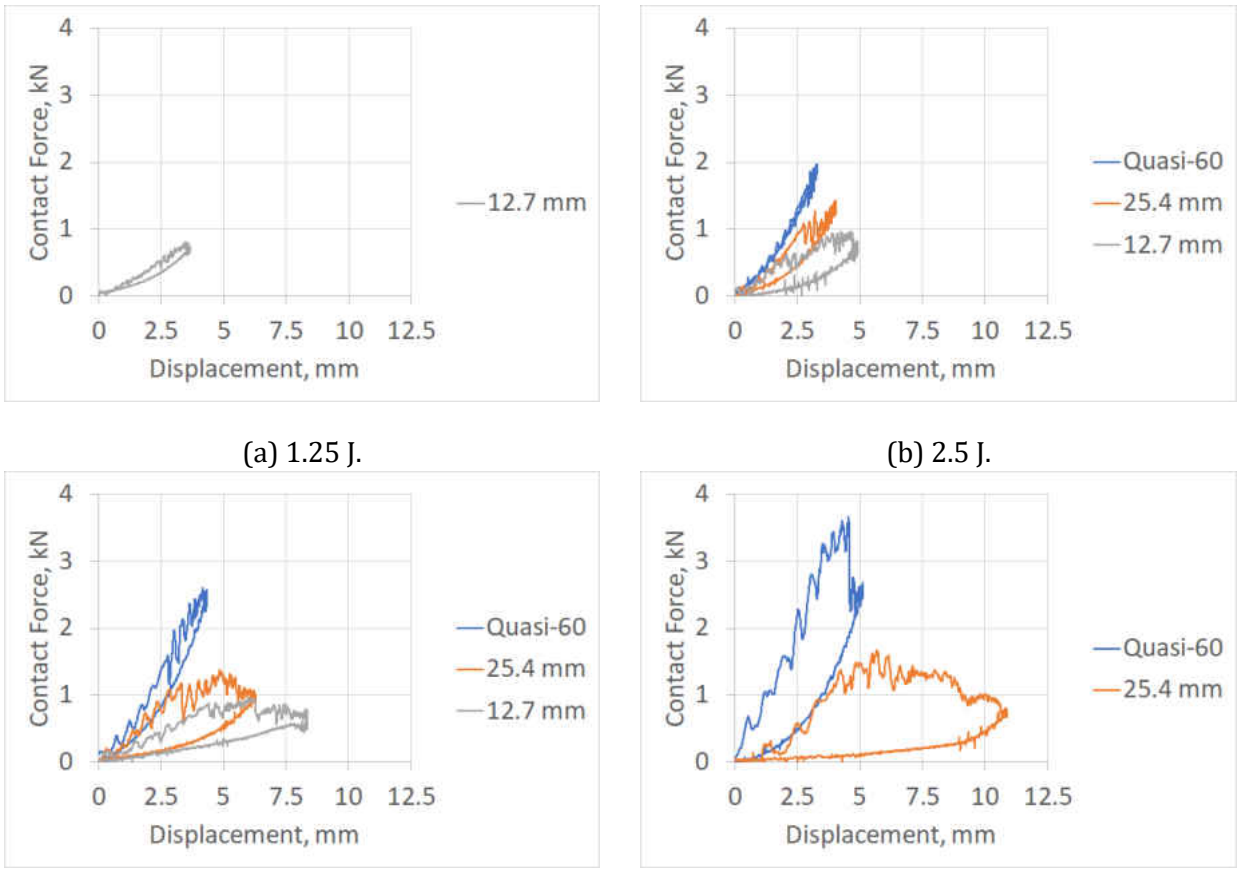

(a) 1.25 J.

(b) 2.5 J.

(c) 5 J.

(d) 10 J.

Fig. 15: Force vs Displacement comparison of materials for all impact energy levels.

The difference in contact loading stiffnesses between materials may have to be explained by the difference in incurred damaged and material differences, which was observed visually in the specimens and experimentally by compression tests after impact, discussed later.

3.3 POST-IMPACT VISUAL ANALYSIS OF THE SAMPLES

Damage in the Quasi-60 material usually presented itself as an indent. Depth was not measured, as it was not in the scope of this experiment, but has been previously explored by other researchers. Higher energies (5 J and 10 J) had a crack at the location of impact. Delamination and general damage were observed using Ultrasonic Testing (UT). At 5 J of impact energy, delaminations on the back of the material were observed in a diamond shape. At 10 J, this backside delamination spread to the edges of the specimen in the direction of the fiber, usually delaminating the two pieces of carbon fiber tape on the back of the specimen.

All specimens failed in 1 of the 5 acceptable failure modes, as defined by the ASTM Standard. Most of the specimens failed laterally through the damage, like the 25.4 mm specimen tested at 2.5 J, as shown in Fig. 16. A UT scan of this specimen is shown in Fig. 16(a), showing little damage (the dark region) in the center of the specimen, propagated to the right. In this specimen, failure occurred laterally in the center, as shown in Fig. 16(b) and 16(c). Arrows are approximately perpendicular to the line of the crack.

The UT before impact testing shows a specimen with several edge delaminations in lighter colors due to cutting, in Fig. 17(a). Another UT was taken after impact, showing the damage due to impact in darker sections in the middle of the specimen, in Fig. 17(b). There is significantly more damage in the 10 J specimen than that of the 2.5 J specimen from Fig. 16(a).

A Computed Tomography scan (CT) showing a 25.4 mm specimen after being impacted with 5 J of energy can be seen in Fig. 18. A planar view is shown in Fig. 18(a) and several cross-sectional views are shown in Fig. 18(b). The center of impact is located at the center

of the specimen. Damage appears to propagate deeper into the specimen and away from the center of impact. The black horizontal line on the left of Fig. 18(a) is a visual artifact of metal shaving occurring as a defect in the manufacturing process.

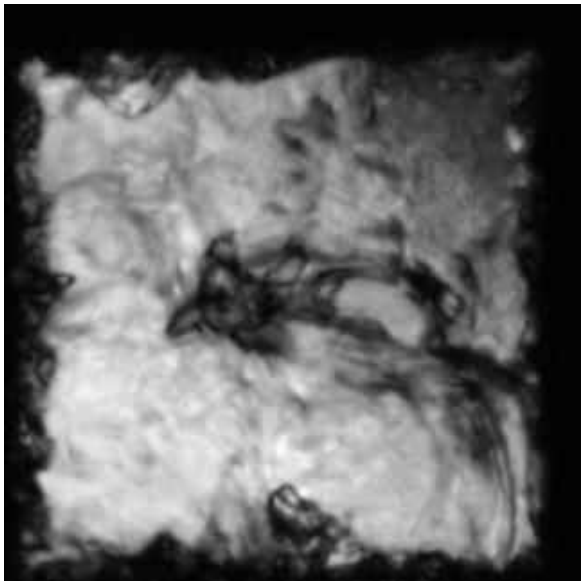

(a) UT.

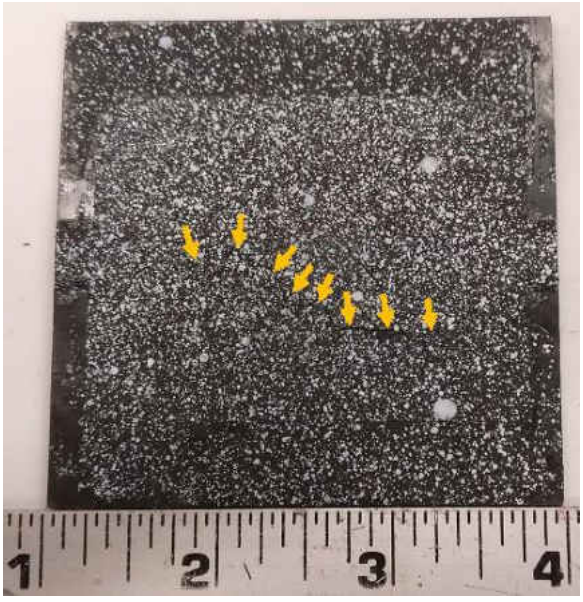

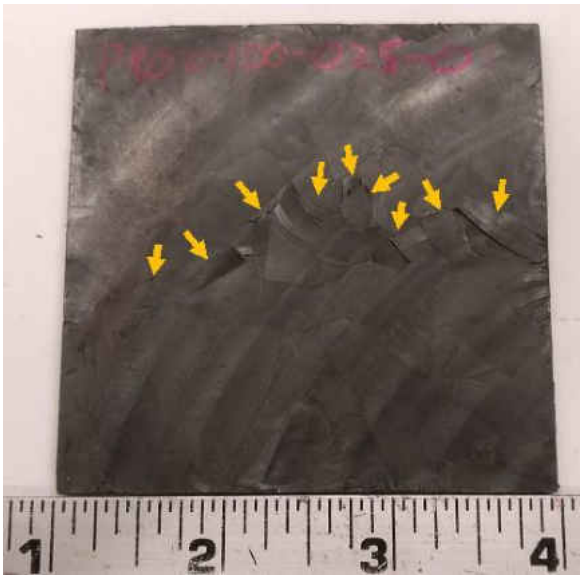

(b) Front. (c) Back.

Fig. 16: Specimen from P902 tested at 2.5 J after compression testing.

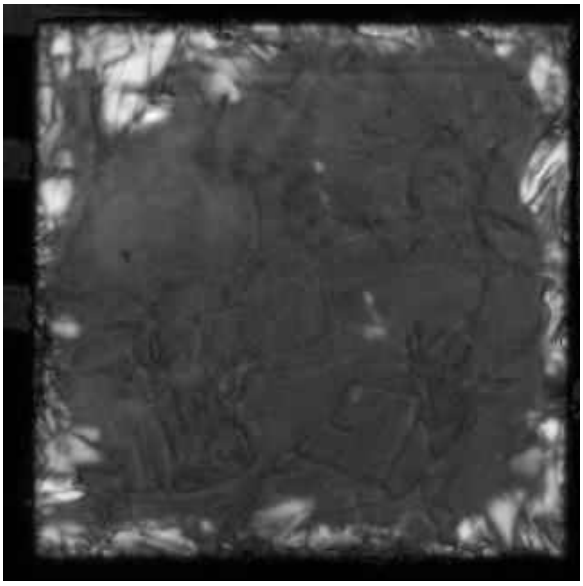

(a) Before impact.

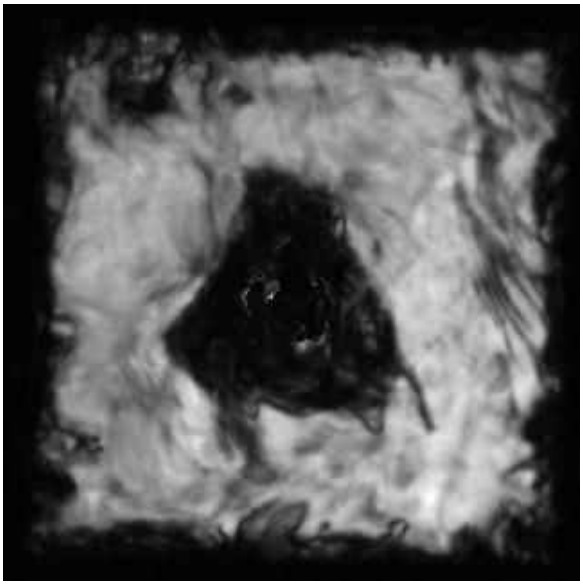

(b) After impact.

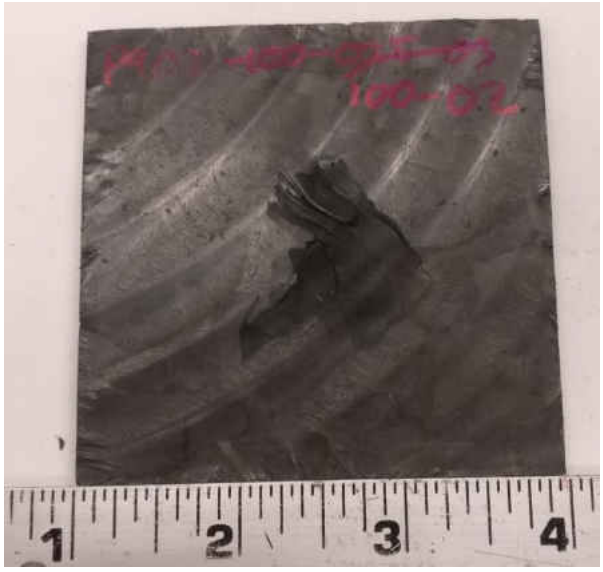

(c) Back of specimen.

(d) Angle showing damage severity.

Fig. 17: Specimen from P902 tested at 10 J.

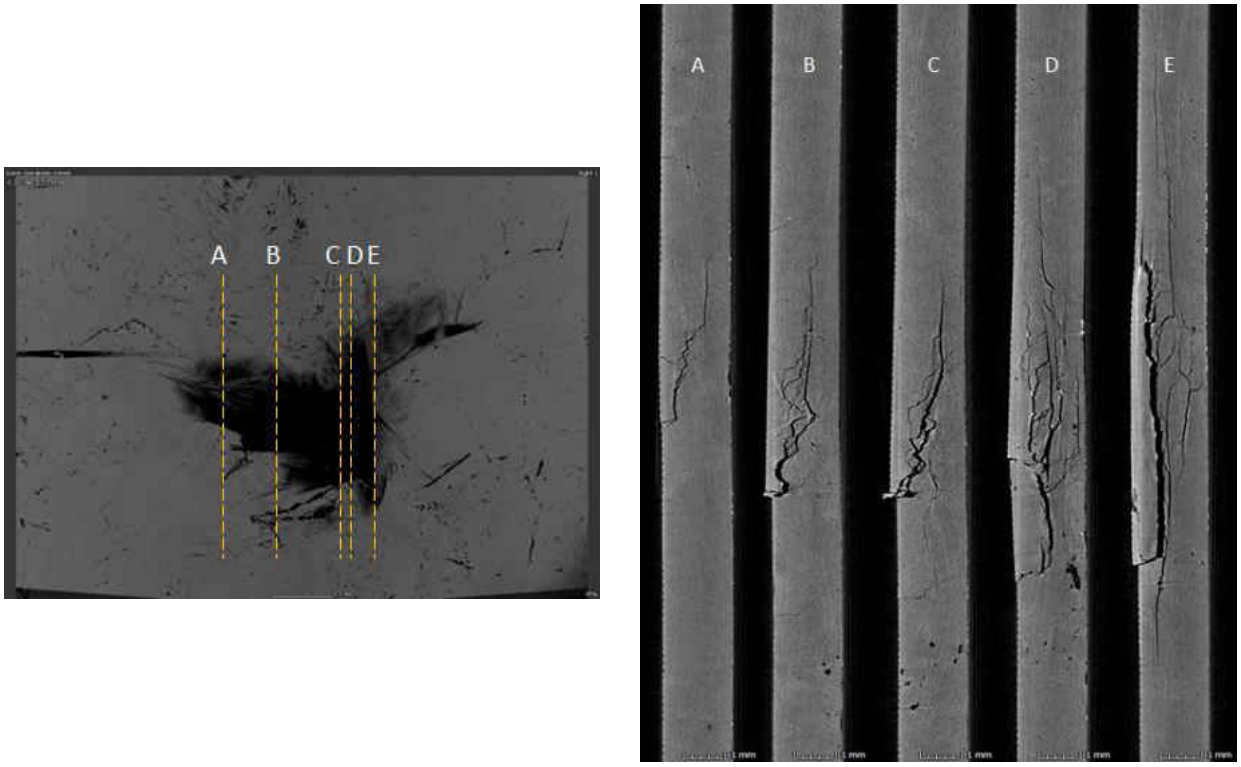

(a) Slice locations. (b) Slices.

Fig. 18: CT of a 25.4 mm specimen tested at 5 J.

3.4 DAMAGE AREA

Papers detailing failure mechanisms due to CAI discuss delamination as a major failure mechanism. The damage area is defined here as the total projected area of damage in the material. Damage area was measured using a C-scan in UT and compared to the total area of the specimen.

Delamination area vs impact energy was explored and the results are presented in Fig. 19. Due to scatter, information was averaged. These values do not use all tested specimens due to missing data. Significant delamination occurred in discontinuous fiber specimens, compared to continuous fiber specimens.

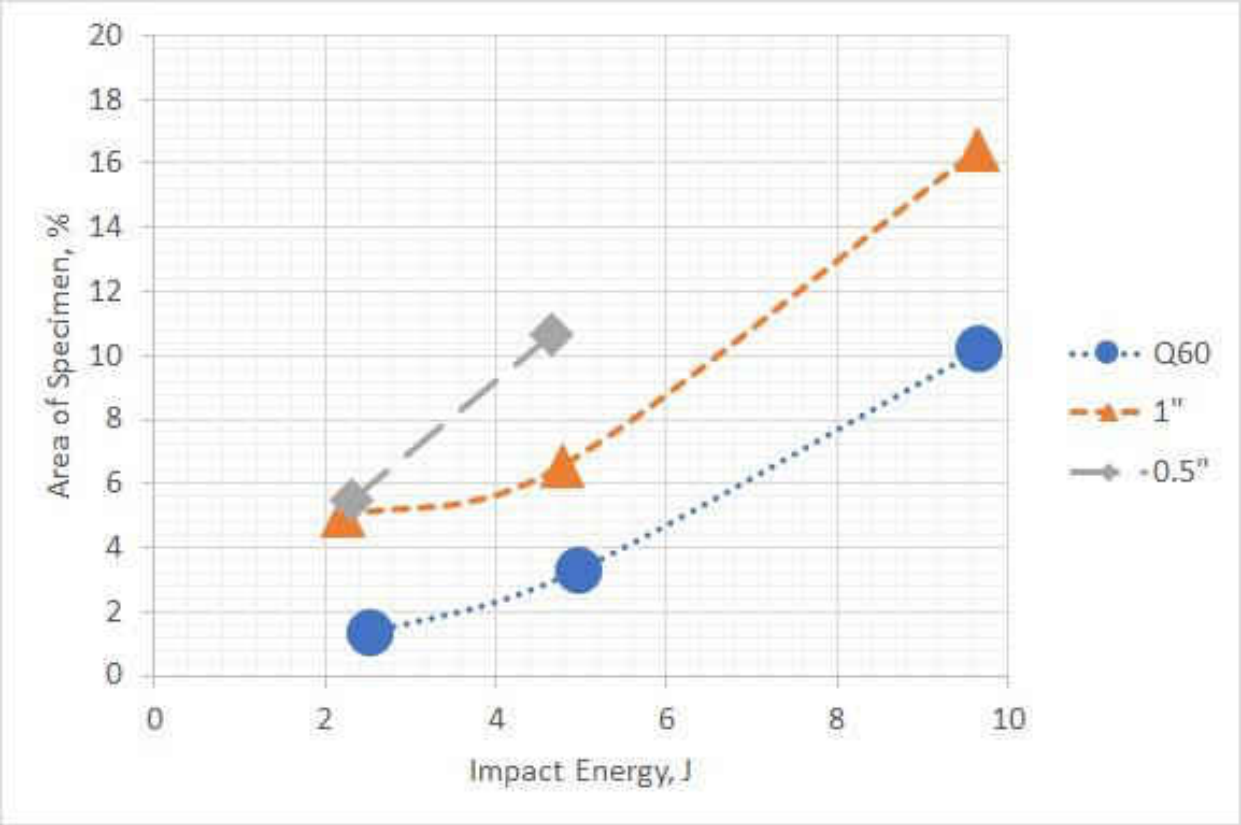

Fig. 19: Delamination area as a percent of total area vs impact energy.

3.5 COMPRESSION

3.5.1 RESIDUAL STRENGTH

Results of all compression and CAI tests are reported in Fig. 20, 21, and 22. Specimens markers with no fill failed under the specimen fixture, or due to buckling of the specimens and were not used in calculations. In each graph, there are two specimen shapes correlating to which panel the specimen was from. Results of each energy level were averaged and are presented in the discussion. All data has been adjusted for recorded impact energies.

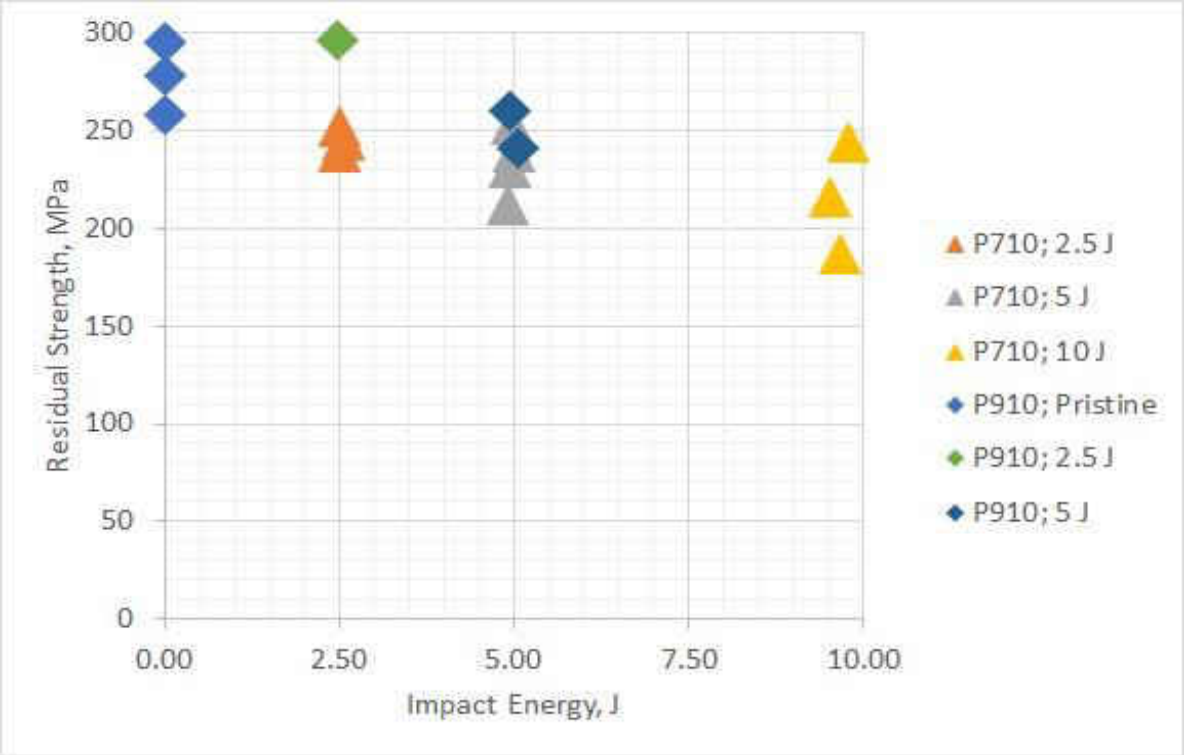

Fig. 20: Quasi-60 data adjusted for actual impact energy.

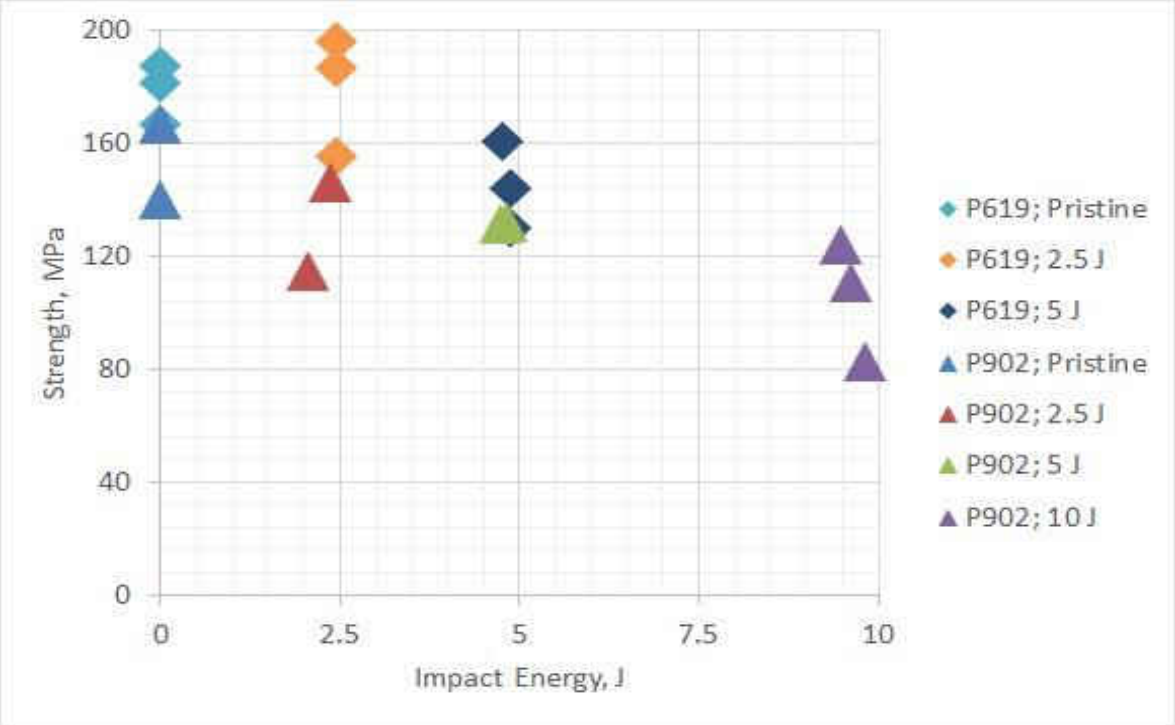

Fig. 21: Data from 25.4 mm platelet panels adjusted for actual impact energy.

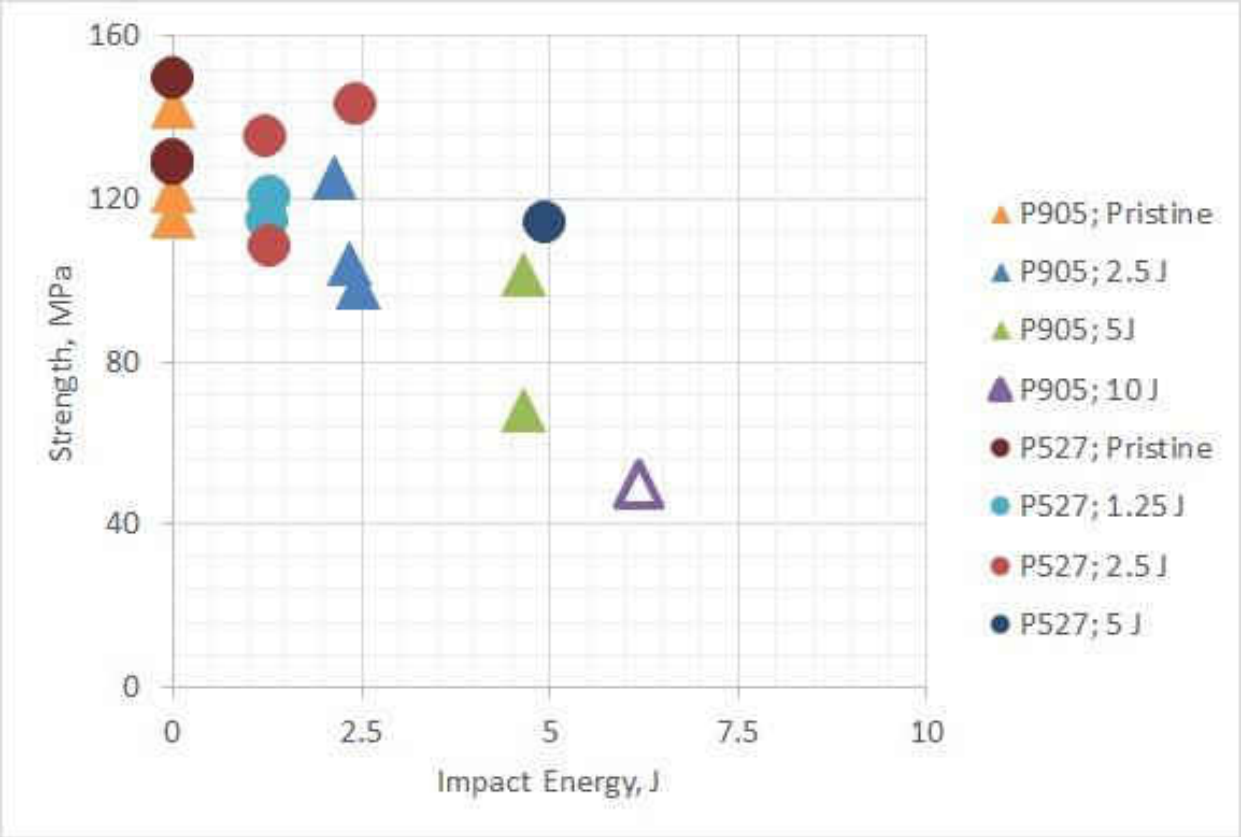

Fig. 22: Data from 12.7 mm platelet panels adjusted for actual impact energy.

3.5.2 STRESS-STRAIN

Stress-strain curves for each material are presented in Fig. 23. Axes are generalized between figures for better comparison of data. Specimens were tested until the final failure resulted in values less than half of the current maximum load.

Strain was calculated from the displacement of the crosshead and the gauge length of the specimen (material height). Modulus was calculated from sections of the stress–strain data where it was constant for at least 0.003 mm/mm. Quasi-60 specimens had the highest modulus of all three materials at around 22.7 GPa, decreasing only around 10 J.

Pristine 25.4 mm specimens had a median modulus value of 9.1 GPa. The modulus decreases with increasing impact energy levels, as seen in Fig. 23(b). This trend is also seen with the 12.7 mm specimens, as shown in Fig. 23(c). Pristine 12.7 mm specimens had an average modulus of 8.5 MPa. It is worth noting the curves become more rounded with decreasing fiber length. The likely reason for this is damage propagation may be easier with shorter fibers due to the inability of the matrix to carry as much load as the fibers. Shorter fibers/platelets would also mean fewer fibers in contact with one platelet, and thus lower surface area for load transfer.

The modulus decreases with increasing impact energies. A comparison of normalized modulus for all three materials is shown in Fig. 24. The discontinuous fiber specimens appear to follow the trend of an upside-down parabola.

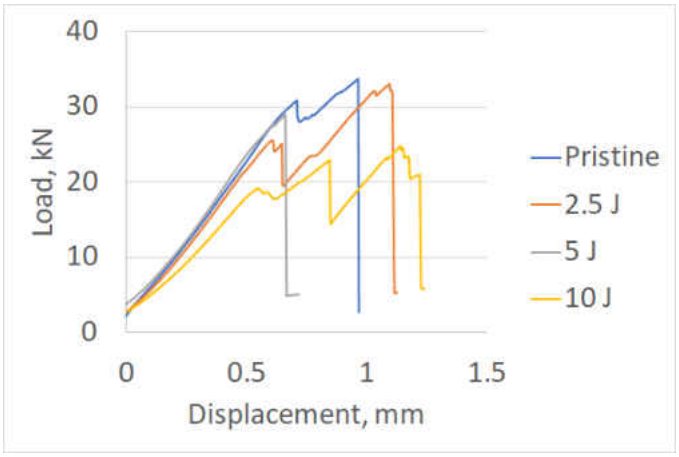

(a) Q60.

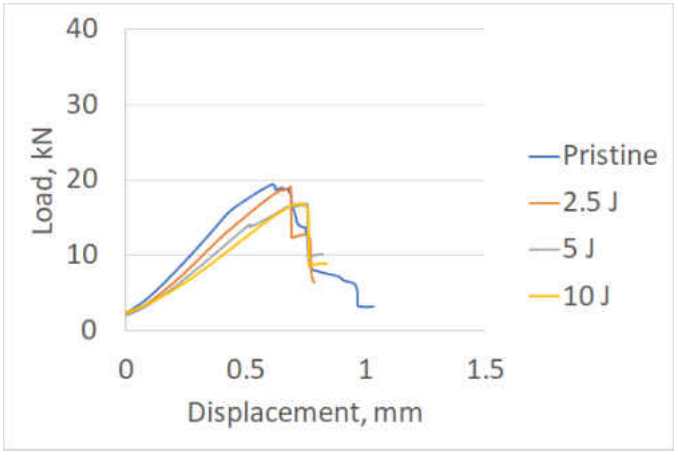

(b) 25.4 mm.

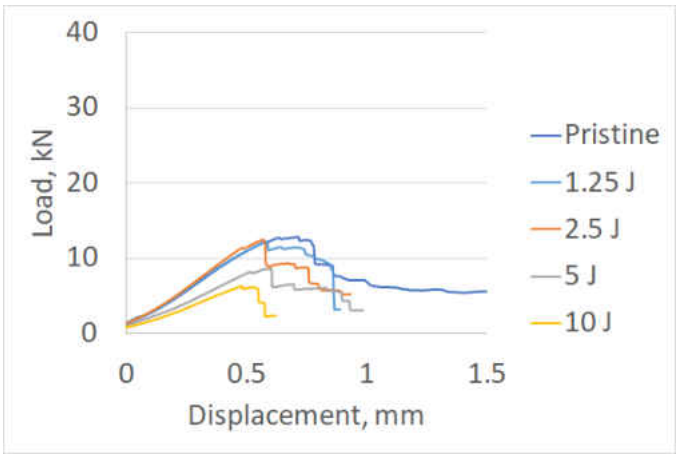

(c) 12.7 mm.

Fig. 23: Stress–strain curves for each material type at all impact energies.

3.6 BUCKLING ANALYSIS

The critical buckling stresses using Eq. 5 for Quasi-60, 25.4 mm, and 12.7 mm materials are 160 MPa, 110 MPa, and 110 MPa, respectively. This calculation used a critical buckling factor of 7 for fixed supports, a Poisson's ratio of 0.3, average material thickness of 1.7 mm, and average specimen width of 76 mm. The moduli can be found in Table III, along with the average experimental strengths and predicted buckling stresses. The Quasi-60 material's predicted critical buckling stress was lower than the average ultimate stress experienced by the material at 277 MPa; however, the 25.4 mm materials' predicted buckling stress was lower than the experienced average ultimate stress of 169 MPa. The 12.7 mm material's buckling stress was below the average maximum stress. The out-of-plane deflections taken at the point just before failure can be seen in Fig. 24.

TABLE III: Buckling values.

Material	Modulus	Experimental Strength	Predicted Buckling Stress
Quasi-60	51 GPa	277 MPa	160 MPa
25.4 mm	35 GPa	169 MPa	110 MPa
12.7 mm	35 GPa	135 MPa	110 MPa

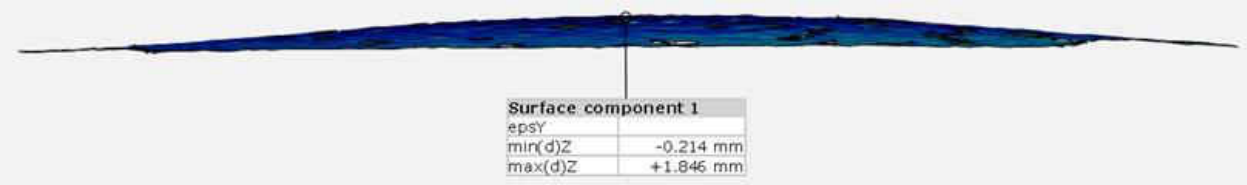

(a) Quasi-60.

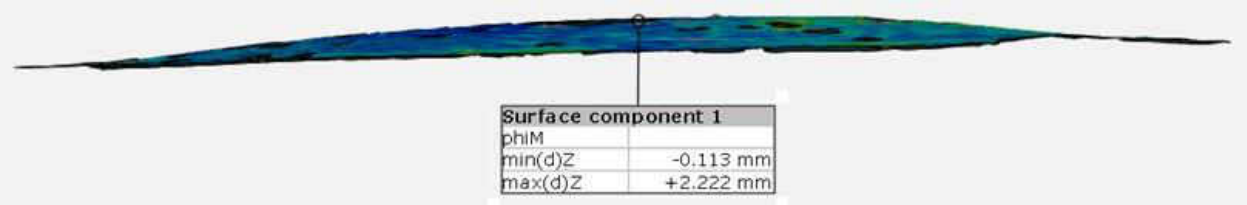

(b) 25.4 mm.

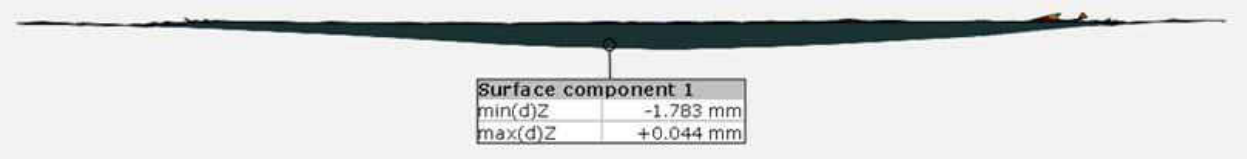

(c) 12.7 mm.

Fig. 24: Out-of-plane deflection of several sample specimens.

3.7 Damage propagation in compression after impact

It was important for the fixture to not interfere with the strength of the damaged composites, so it was designed with a large window. Because of this, DIC was made possible. In this section, DIC of several specimens at various energy levels will be presented, along with general trends observed. Load vs displacement curves, UTs, and interesting stages of DIC are presented. The DIC shown is an Equivalent Mises Strain, chosen in order to show the total deformation in the specimen. This strain is always positive. The scale shown ranges from 0% to 6% strain. Extremes in the strain (strain greater than 6% are represented by either a maroon or white patch, and typically represent either crack/delamination formation or portions of the paint which have flecked off the specimen (usually due to crack/delamination formation). Images were captured at a rate of 1 Hz. Two Quasi-60

specimens can be seen in Fig. 25. The pristine specimen can be found in Fig. 25(a), 25(b), 25(c), while the specimen impacted with 5 J is found in Fig. 25(d), 25(e), 25(f). The two stages of DIC presented for each specimen are one immediately before fracture, and one immediately after. Pristine specimens of the Quasi-60 material failed in one of two ways. Either no cracks formed until sudden catastrophic failure, as shown in Fig. 25(b) and Fig. 25(c), or several initiation points across the center of the specimen propagated until the cracks merged at catastrophic failure of the specimen. Little surface fracture is observed on the DIC side of this specimen, though a fracture through a majority (95%) of the fibers on the rear surface is visible.

All impacted specimens failed in the same manner, propagating a damage in the center created at the time of impact from the center to the edges of the specimen, as shown in Fig. 25(f) and Fig. 25(f).

Similar to pristine Quasi-60 specimens, most pristine, discontinuous fiber specimens had several crack-initiation points that connected at, around, or after catastrophic failure. An example of this behavior can be seen in Fig. 26. Catastrophic failure occurs between Fig. 26(c) and Fig. 26(d).

An impacted specimen for the 25.4 mm material is shown in Fig. 27. This figure contains a load vs displacement graph, UT after impact, and four stages of DIC. Catastrophic failure occurs between Fig. 27(d) and Fig. 27(e). The final stage in the DIC of this test is given for reference of crack propagation. As with most of the damaged specimens, cracks begin at the location of impact and spread to the edges. Cracks appeared to follow platelet edges, but generally appeared to propagate in more smooth, arcing methods.

It may be important to note the damaged areas in Fig. 27(b) (dark portions in the center of the specimen) are in a similar pattern to the strain towards the right in Fig. 27(e). A projection was not used when creating the DIC images, and given the angled capture of the DIC rotated to be normal to the viewer, locations may not line up to actual locations on the specimen.

Another example of deformations revealed by the DIC having a similar pattern to the damage area observed in UT can be seen with a 12.7 mm specimen in Fig. 28. The comparison is best made between the UT in Fig. 28(b) and the DIC in Fig. 28(c). The load–displacement curve is presented in Fig. 28(a), with DIC stages of interest given later in the figure.

The impact damaged the surface of this specimen, leaving a short crack on the surface. During compression testing, cracks propagated from this point to combine with cracks formed at the edges of the specimen. Most 12.7 mm specimens contained erratic or jagged crack propagation, seemingly following platelet edges.

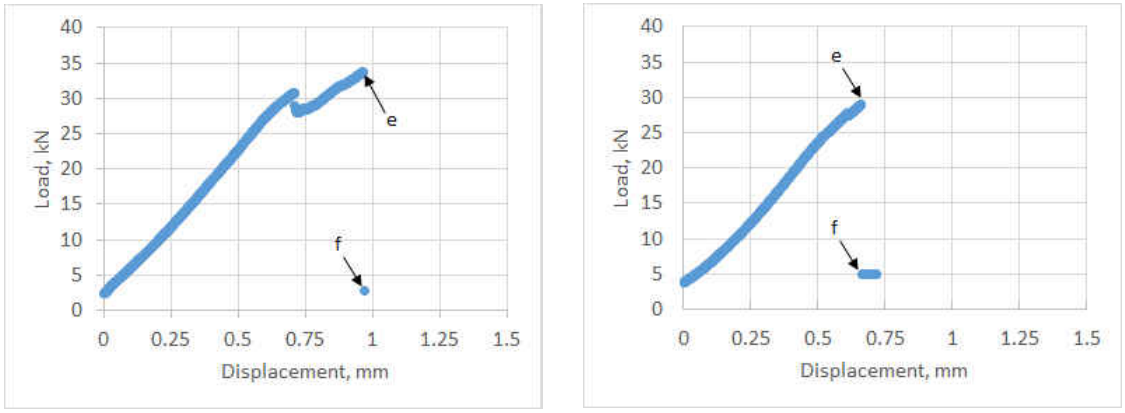

(a) Load vs Displacement. (d) Load vs Displacement.

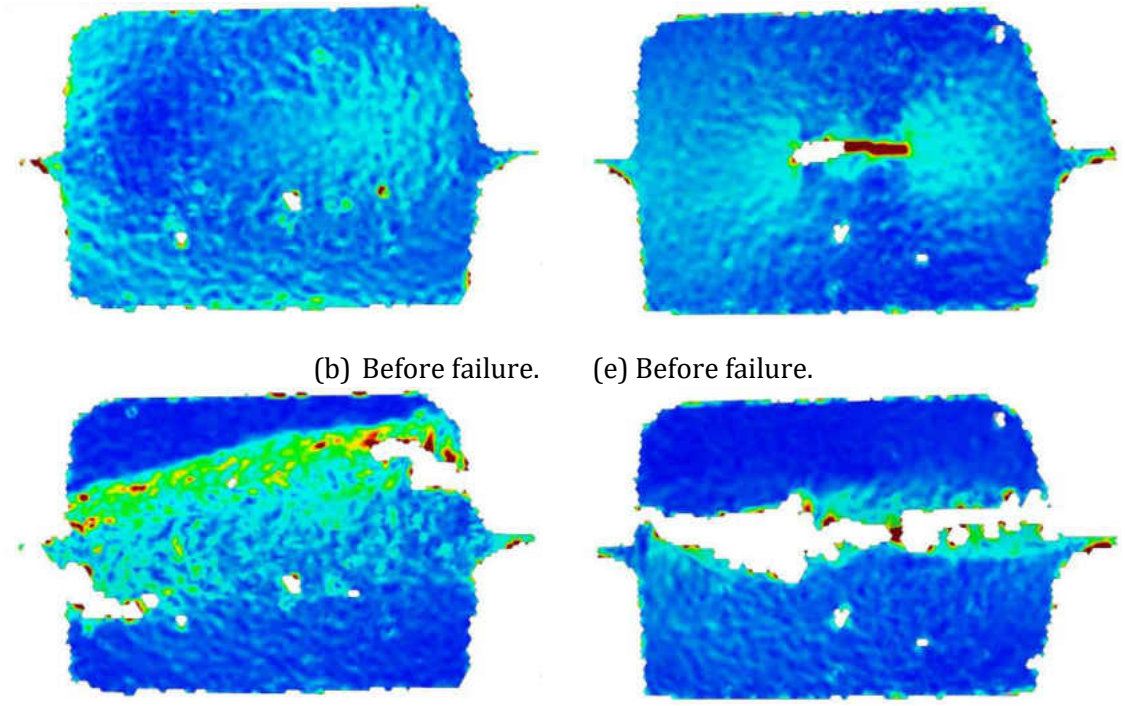

(b) Before failure. (e) Before failure.

(c) After failure. (f) After failure.

Fig. 25: DICs of pristine (left) and impacted (right) Quasi-60 specimens. The damaged specimen was impacted with 5 J of energy.

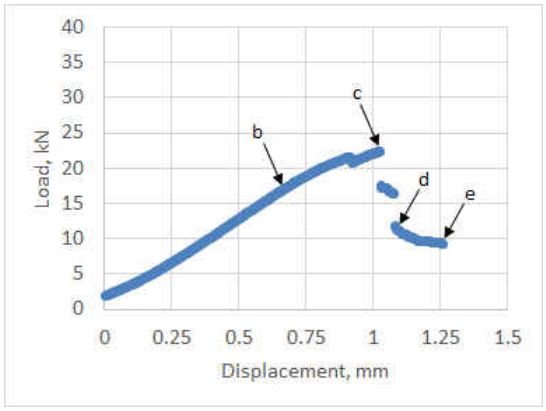

(a) Stress vs Strain.

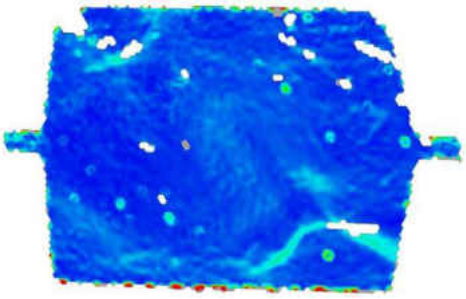

(b)

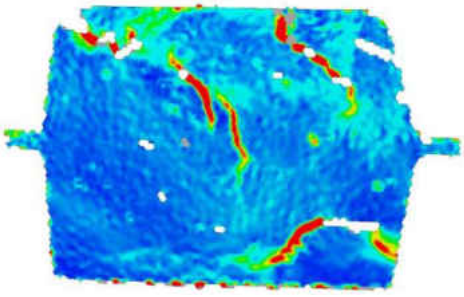

(c)

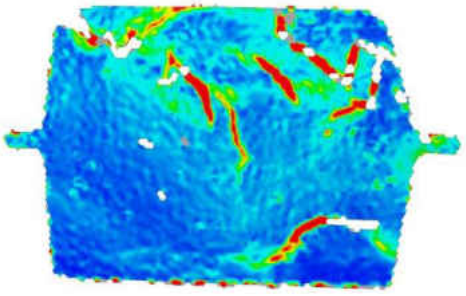

(d)

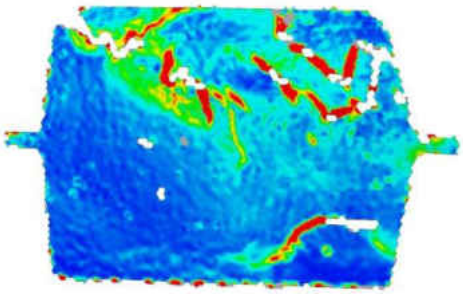

(e)

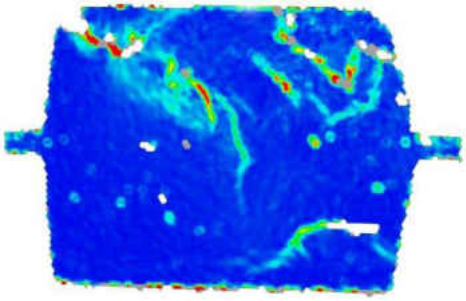

(f)

Fig. 26: DIC of a pristine 25.4 mm specimen.

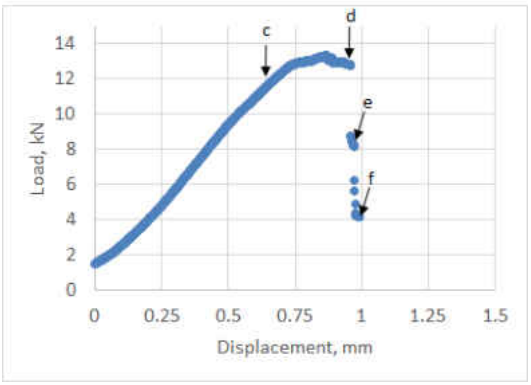

(a) Stress vs Strain.

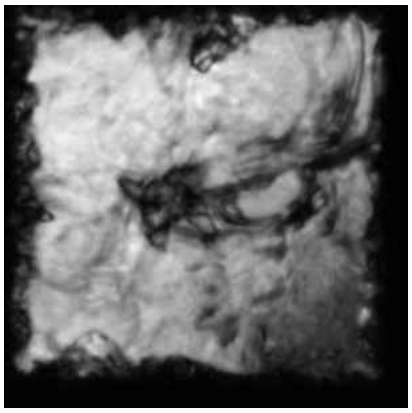

(b) UT.

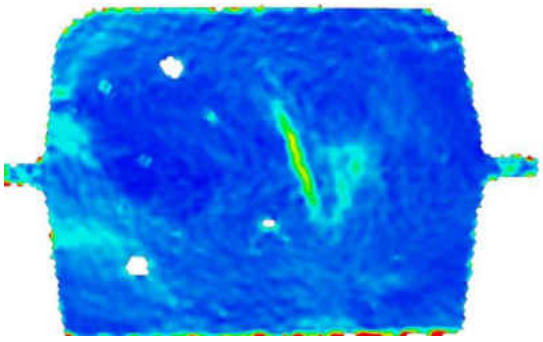

(c)

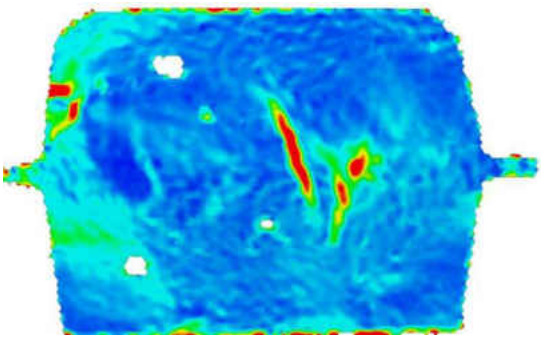

(d)

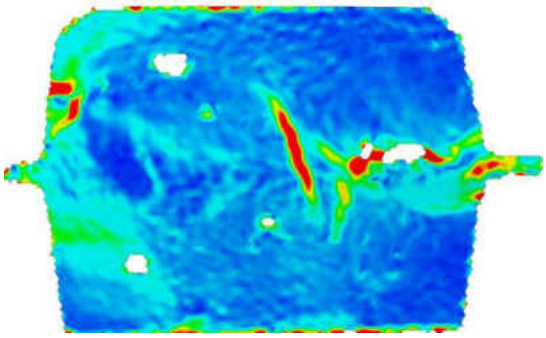

(e)

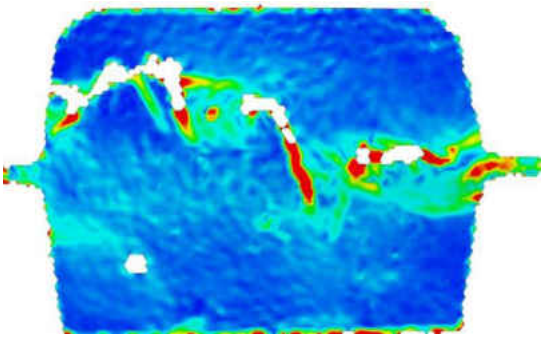

(f)

Fig. 27: DIC of a 25.4 mm specimen impacted with 2.5 J of energy.

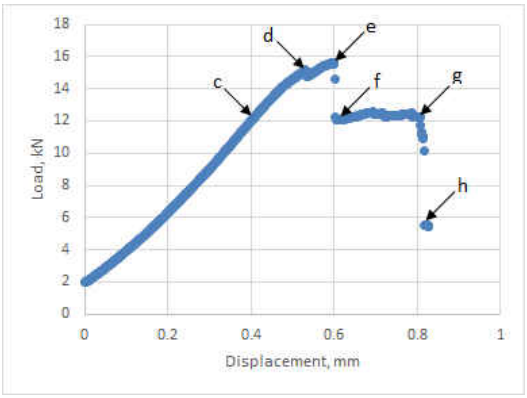

(a) Stress vs strain.

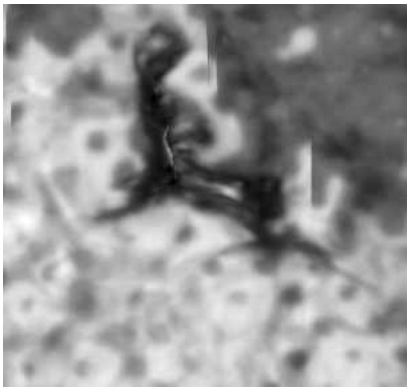

(b) UT.

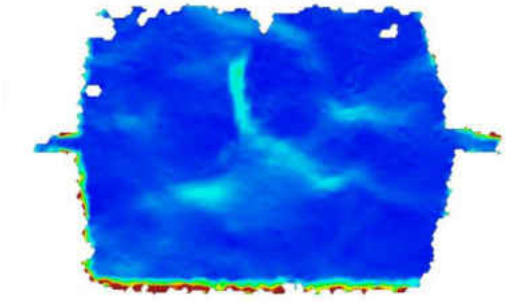

(c)

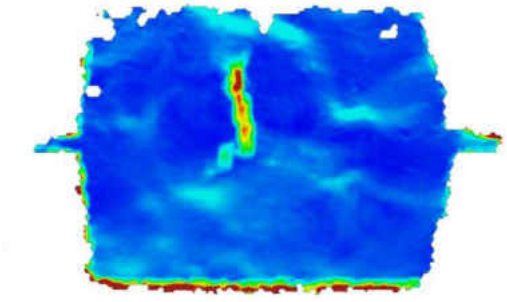

(d)

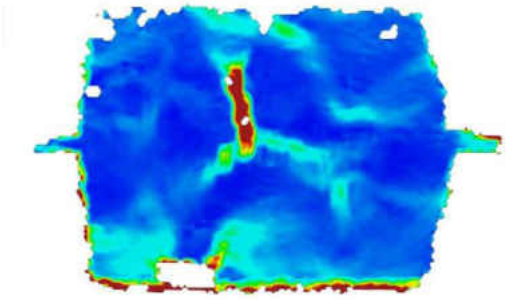

(e)

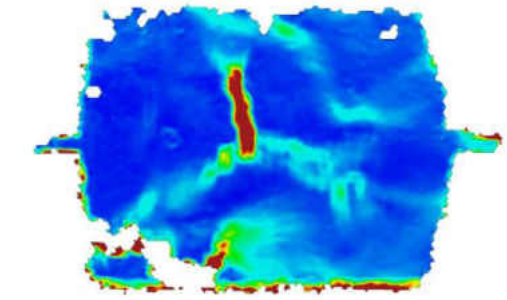

(f)

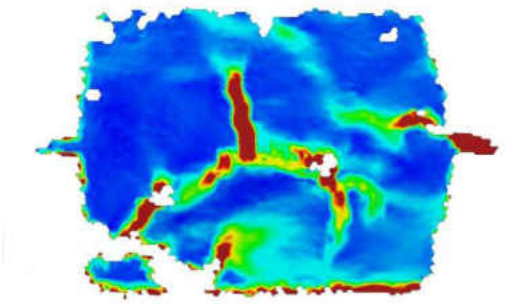

(g)

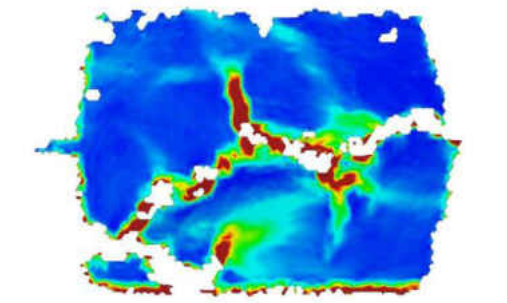

(h)

Fig. 28: DIC of a 12.7 mm specimen impacted with 2.5 J of energy.

3.8 DISCUSSION

Values from Fig. 20, 21, and 22 have been averaged and are presented in Fig. 29. A downward trend with a similar slope is observed for all three materials. In order to compare how much of the original strength is lost in CAI of these materials, each residual strength was normalized to the pristine strength of the specimen, and is presented in Fig. 30. Error bars indicate maximum/minimum values, due to few data points.

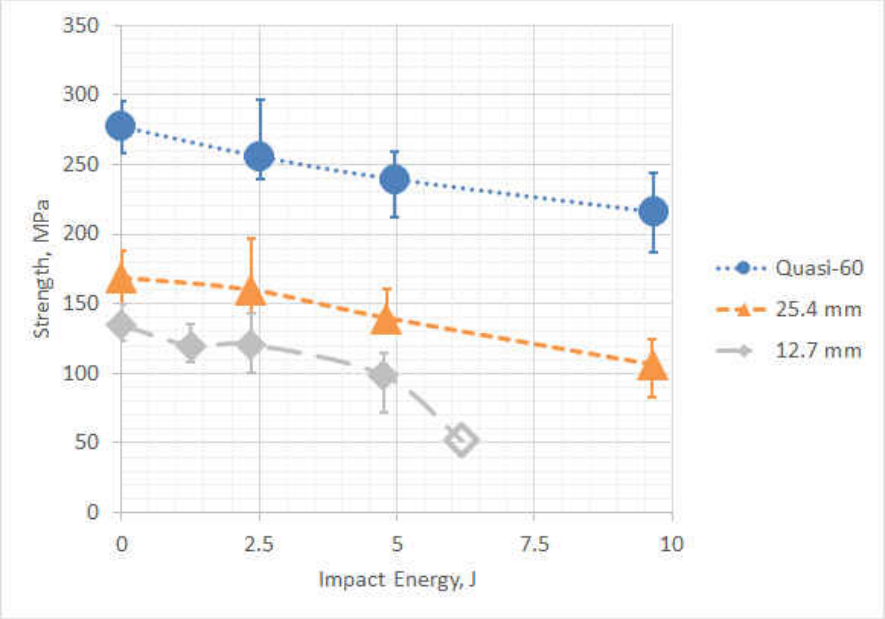

Fig. 29: Average residual strengths for all materials. Values adjusted for actual recorded impact energy.

As observed in Fig. 29, 30, residual strength appears to decrease with decreasing fiber length. An impact energy of 2.5 J appears to effect all materials similarly, giving a residual strength at 92±5% for all. For reference, the Sanchez-Saez paper found an 80% residual strength for their Quasi-45 impacted at 2.5 J and approximately 71% at 5 J [24]. At 5 J, results begin to spread out. The 12.7 mm specimen could not withstand 10 J of

impact energy as the impactor punctured the material, but the specimen is presented regardless.

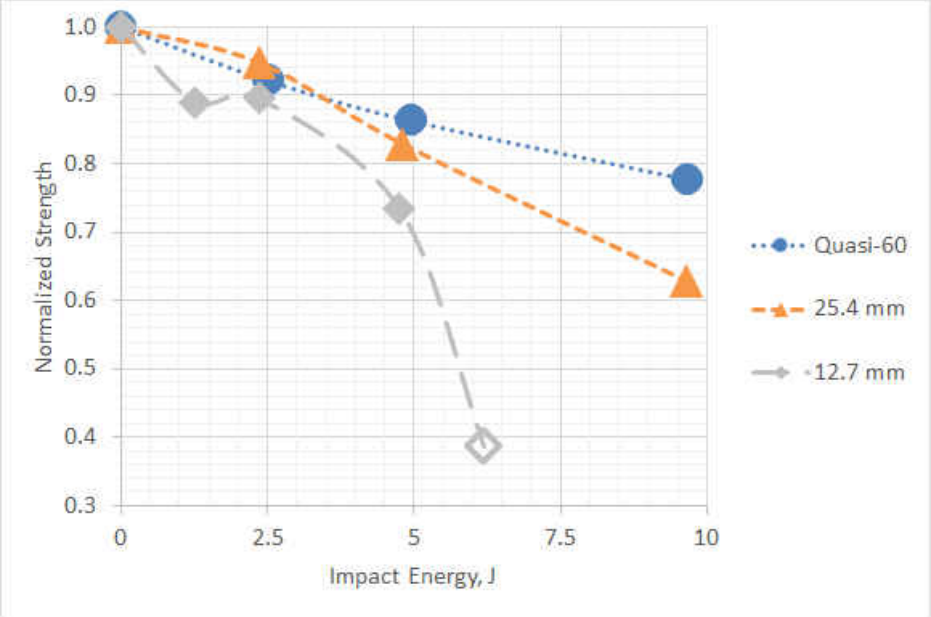

Fig. 30: Normalized residual strength for all materials. Values adjusted for actual recorded impact energy.

The normalized stiffness is shown for all materials in Fig. 31. This stiffness is calculated from the MTS crosshead displacement. The discontinuous fiber materials decrease similar to an open-end-down parabola, while the continuous fiber material had a more erratic trend downwards, similar to strength.

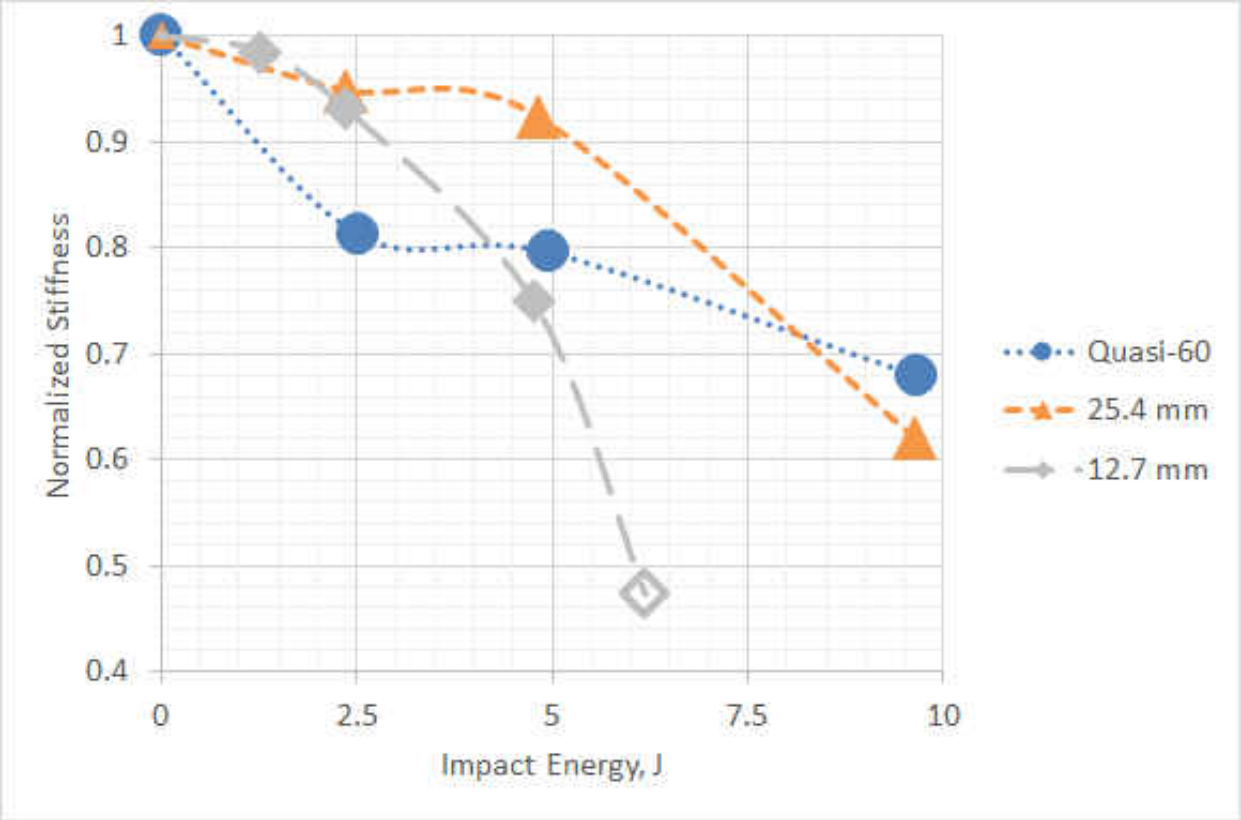

Fig. 31: Normalized Modulus for all tested materials.

It was determined the standard deviation was not a good representative for a low quantity of data. Therefore, the coefficient of variation was explored using the range of the data at a given energy level. These are presented at the intended impact energy level in Fig. 32. The coefficient of variation appeared to increase with increasing impact energy, but no conclusions can be made due to the fluctuation in the coefficient.

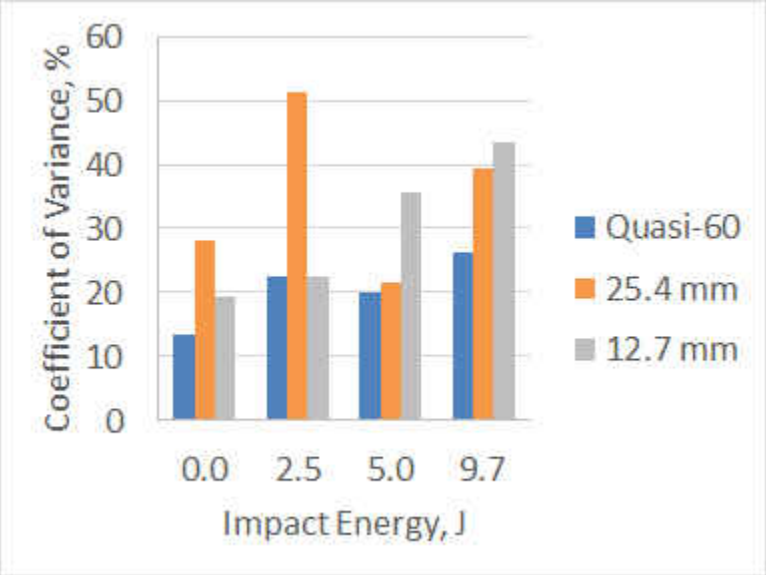

Fig. 32: Coefficient of Variation using the ranges of the sample sets

CHAPTER 4

CONCLUDING REMARKS

Two different prepreg platelet molded composites with stochastic morphologies were tested to determine the residual strength due to compression after impact. A Quasi-60 layup was used as a control for the experiment. The three materials were impact-tested at 4 impact energies. Residual strengths were averaged and normalized to determine the residual strength of the composites, which was found to decrease with increasing impact energy. The residual strength was also found to decrease with decreasing fiber length. For Quasi-60, the final DIC of several specimens were presented. Post-impact, pre-compression UT's and load–displacement curves were presented for these specimens. Crack propagation randomness decreased with increasing fiber length. Crack initiation for pristine specimens was random, eventually connecting at catastrophic failure. Impacted specimens contained cracks that propagated from the center of the specimen to the specimen's edge.

4.1 RELATED WORK

The work in this thesis provides the groundwork for further research in areas related to prepreg platelet molded composites. The first area of recommended research is to develop a better fixture for 1.7mm composites. Some improvements have been made to the ASTM Standard, but these results have been marginally successful for especially thin materials. A larger specimen may be necessary due to widespread damage within the material. It is possible the cracks make a difference in the strength of the material if the damage is too close to the edges of the specimen, making it less representative of real applications.

After testing a fixture, it would be ideal to make sure no step of the manufacturing process has an effect on the properties of the material; for example, the platelets tend to bunch up and stick together when cut from the tape. This may cause directional properties, pockets of strength or weakness, etc. This may help with the material variability, though it is not expected. Post-compression UT and CT would allow observation of damage propagation and possible failure modes.

Computational and 3D modeling and simulation may provide better insights as to the behavior of these materials, paving the way for inclusion in engineering analysis of structures.

This would also allow development of better test methods.

Changing platelet length also changed the ultimate strength. It is known that variations in width or thickness of the platelet will change the ultimate strength, so further exploration of the role of the platelet size effect on the residual stress after impact is necessary. It would be recommended to complete this testing after modeling of current work. If the model works for variations of a single parameter, it should ideally be representative of variations in other parameters.

REFERENCES

[1] R. B. Seymour and R. Deanin, *History of polymeric composites*. VNU science press, 1987.

[2] B. R. Denos, D. E. Sommer, A. J. Favaloro, R. B. Pipes, and W. B. Avery, "Fiber orientation measurement from mesoscale ct scans of prepreg platelet molded composites," *Composites Part A: Applied Science and Manufacturing*, vol. 114, pp. 241 – 249, 2018.

[3] P. Feraboli, E. Peitso, F. Deleo, T. Cleveland, and P. B. Stickler, "Characterization of prepreg-based discontinuous carbon fiber/epoxy systems," *Journal of Reinforced Plastics and Composites*, vol. 28, no. 10, pp. 1191–1214, 2008.

[4] P. Feraboli, E. Peitso, T. Cleveland, and P. B. Stickler, "Modulus measurement for prepreg-based discontinuous carbon fiber/epoxy systems," *Journal of Composite Materials*, vol. 43, no. 19, pp. 1947–1965, 2009.

[5] S. G. Kravchenko, D. E. Sommer, and R. B. Pipes, "Uniaxial strength of a composite array of overlaid and aligned prepreg platelets," *Composites Part A: Applied Science and Manufacturing*, vol. 109, pp. 31 – 47, 2018.

[6] S. G. Kravchenko, D. E. Sommer, B. R. Denos, A. J. Favaloro, C. M. Tow, W. B. Avery, and R. B. Pipes, "Tensile properties of a stochastic prepreg platelet molded composite," *Composites Part A: Applied Science and Manufacturing*, vol. 124, p. 105507, 2019.

[7] S. Ko, J. Yang, M. E. Tuttle, and M. Salviato, "Effect of the platelet size on the fracturing behavior and size effect of discontinuous fiber composite structures," *Composite Structures*, vol. 227, p. 111245, 2019.

[8] "Car Accident Statistics in LA — fisher talwar 2020," 2020.

[9] "NHTSA report 2020." https://one.nhtsa.gov/nhtsa/whatis/planning/2020Report/2020report.html, Sept 1997. Accessed on 2020-02-20.

[10] W. Cantwell and J. Morton, "The impact resistance of composite materials a review," *Composites*, vol. 22, no. 5, pp. 347–362, 1991.

[11] P. O. Sjoblom, J. T. Hartness, and T. M. Cordell, "On low-velocity impact testing of composite materials," *Journal of Composite Materials*, vol. 22, no. 1, pp. 30–52, 1988.

[12] J. Winkel and D. Adams, "Instrumented drop weight impact testing of cross-ply and fabric composites," *Composites*, vol. 16, no. 4, pp. 268–278, 1985.

[13] S. Bernhardt, M. Ramulu, and A. S. Kobayashi, "Low-Velocity Impact Response Characterization of a Hybrid Titanium Composite Laminate," *Journal of Engineering Materials and Technology*, vol. 129, pp. 220–226, 07 2006.

[14] D. Ghelli and G. Minak, "Low velocity impact and compression after impact tests on thin carbon/epoxy laminates," *Composites Part B: Engineering*, vol. 42, no. 7, pp. 2067 – 2079, 2011.

[15] W. Tan, B. G. Falzon, L. N. Chiu, and M. Price, "Predicting low velocity impact damage and compression-after-impact (cai) behaviour of composite laminates," *Composites Part A: Applied Science and Manufacturing*, vol. 71, pp. 212 – 226, 2015.

[16] M. de Freitas and L. Reis, "Failure mechanisms on composite specimens subjected to compression after impact," *Composite Structures*, vol. 42, no. 4, pp. 365 – 373, 1998.

International Workshop on Experimental Techniques in the Analysis of Composite Structures.

[17] R. Prabhakaran, "Tensile fracture of composites with circular holes," *Materials Science and Engineering*, vol. 41, no. 1, pp. 121 – 125, 1979.

[18] S. L. Chang, Yau and T. Chou, "Notched strength of woven fabric composites with moulded-in holes," *Composites*, vol. 18, no. 3, pp. 233–241, 1987.

[19] T. OBRIEN and I. RAJU, *Strain-energy-release rate analysis of delamination around an open hole in composite laminates*.

[20] J. W. Mar and K. Y. Lin, "Fracture mechanics correlation for tensile failure of filamentary composites with holes," *Journal of Aircraft*, vol. 14, no. 7, pp. 703–704, 1977.

[21] S. D. Pandita, K. Nishiyabu, and I. Verpoest, "Strain concentrations in woven fabric composites with holes," *Composite Structures*, vol. 59, no. 3, pp. 361 – 368, 2003.

[22] "Standard test method for compressive residual strength properties of damaged polymer matrix composite plates," 2017.

[23] M. Remacha, S. Sa´nchez-Sa´ez, B. Lo´pez-Romano, and E. Barbero, "A new device for determining the compression after impact strength in thin laminates," *Composite Structures*, vol. 127, pp. 99 – 107, 2015.

[24] S. Sanchez-Saez, E. Barbero, R. Zaera, and C. Navarro, "Compression after impact of thin composite laminates," *Composites Science and Technology*, vol. 65, no. 13, pp. 1911 – 1919, 2005.

[25] G. Davies, D. Hitchings, T. Besant, A. Clarke, and C. Morgan, "Compression after impact strength of composite sandwich panels," *Composite Structures*, vol. 63, no. 1, pp. 1 – 9, 2004.

[26] D. Rees, *Appendix B: Plate Buckling Under Uniaxial Compression*, pp. 525–535. 10 2009.

[27] T. Wierzbicki, "Structural mechanics," 2013.

[28] "Ssrc guide to stability design criteria for metal structures," 2009.

[29] Hexcel 8552 IM7 Material Property Data Report. April 22, 2011.

VITA

Christopher Eugene Ervin Volle
Department of Mechanical and Aerospace Engineering
Old Dominion University
Norfolk, VA 23529

Education
Bachelors of Science in Mechanical Engineering. Department of Mechanical Engineering, University of Nebraska - Lincoln, Lincoln, Nebraska. December 2016.

Publications
Hawbaker, James; Koenig, John; Volle, Christopher; Glass, David E.; Weller, Leslie; and Sullivan, Brian: In-Plane Biaxial Testing and Stress Interaction of a QuasiIsotropic Carbon-Carbon Composite, 37th JANNAF Airbreathing Propulsion Subcommittee Meeting. Dayton, OH, June 3-7, 2019.

Volle, Christopher E. E.; Glass, David E.; Vaughn, Wallace L.: Modeling a CARBON/CARBON Textile Composite under Biaxial Cyclic Tension Loading, 36th JANNAF Airbreathing Propulsion Subcommittee Meeting. Newport News, VA, Dec, 2017.

Presentations
Comparison of Biaxial Continuum Damage Mechanics Model with Test Data for Advanced Carbon-Carbon-6. 43rd USACA Annual Conference on Composites, Materials, and Structures. January 2018.

Modeling a CARBON/CARBON Textile Composite under Biaxial Cyclic Tension Loading. 42nd United States Advanced Ceramics Association (USACA) Annual Conference on Composites, Materials, and Structures. January 2017.

Awards
USIP SFRO Research Grant Recipient, $200,000, 2016.
Boundless Aspirations in Merit and Fellowship Award, Aerospace Club, 2015-2016.
NASA Nebraska Fellow, $4000, 2015-2016.
NASA Nebraska Space Grant Recipient, $6000, 2014-2016.

Typeset using LATEX.